

ASTROMETRIC LIMITS ON THE STOCHASTIC GRAVITATIONAL WAVE BACKGROUND

JEREMY DARLING,¹ ALEXANDRA E. TRUEBENBACH,¹ AND JENNIE PAIN¹

¹Center for Astrophysics and Space Astronomy
 Department of Astrophysical and Planetary Sciences
 University of Colorado, 389 UCB
 Boulder, CO 80309-0389, USA

Submitted to ApJ

ABSTRACT

The canonical methods for gravitational wave detection are ground- and space-based laser interferometry, pulsar timing, and polarization of the cosmic microwave background. But as has been suggested by numerous investigators, astrometry offers an additional path to gravitational wave detection. Gravitational waves deflect light rays of extragalactic objects, creating apparent proper motions in a quadrupolar (and higher order modes) pattern. Astrometry of extragalactic radio sources is sensitive to gravitational waves with frequencies between roughly 10^{-18} and 10^{-8} Hz (H_0 and $1/3 \text{ yr}^{-1}$), overlapping and bridging the pulsar timing and CMB polarization regimes. We present methodology for astrometric gravitational wave detection in the presence of large intrinsic uncorrelated proper motions (i.e., radio jets). We obtain 95% confidence limits on the stochastic gravitational wave background using 711 radio sources, $\Omega_{GW} < 0.0064$, and using 508 radio sources combined with the first *Gaia* data release: $\Omega_{GW} < 0.011$. These limits probe gravitational wave frequencies $6 \times 10^{-18} \text{ Hz} \lesssim f \lesssim 1 \times 10^{-9} \text{ Hz}$. Using a WISE-*Gaia* catalog of 567,721 AGN, we predict a limit expected from *Gaia* alone of $\Omega_{GW} < 0.0006$, which is significantly higher than originally forecast. We incidentally detect and report on 22 new examples of optical superluminal motion with redshifts 0.13–3.89.

Keywords: astrometry — cosmology: observations — gravitational waves — inflation — proper motions — techniques: high angular resolution

1. INTRODUCTION

A stochastic gravitational wave background deflects light from distant objects, producing an apparent proper motion (Braginsky et al. 1990). The angular deflections will be correlated across the sky with amplitude of order the dimensionless strain of the gravitational waves, h_{rms} (Braginsky et al. 1990; Kaiser & Jaffe 1997); one microarcsecond (μas) of deflection is equivalent to a dimensionless strain $h \sim 5 \times 10^{-12}$. Observations spanning a time interval $\Delta t = 1/f_{obs}$ will be sensitive to gravitational waves with frequencies $f < f_{obs}$, roughly down to the inverse of the light travel time to the observed objects, $f \sim 10^{-18}\text{--}10^{-17}$ Hz (e.g., Book & Flanagan 2011).

Book & Flanagan (2011) show that the cosmological gravitational wave background energy density can be related to the correlated light deflections as

$$\Omega_{GW}(f) \sim \langle \mu(f)^2 \rangle / H_0^2, \quad (1)$$

where $\langle \mu(f)^2 \rangle$ is the variance in the proper motion at observed frequency f , and H_0 is the Hubble constant. The proper motion power spectrum, for quadrupolar and higher-order modes, can measure or constrain the gravitational wave background over ten decades in frequency, $H_0 \lesssim f \lesssim 1 \text{ yr}^{-1}$ ($10^{-18} \lesssim f \lesssim 10^{-8}$ Hz). The dominant signal is quadrupolar (Fig. 1), with smaller contributions from $\ell > 2$ modes. In practice, observations constrain the energy density integrated over frequencies, $\int \Omega_{GW}(f) d \ln f$, which will hereafter be labeled as Ω_{GW} .

Detecting or constraining $\sim 10^{-18}\text{--}10^{-16}$ Hz primordial gravitational waves is a key goal of CMB polarization B-mode measurements (e.g., Kamionkowski et al. 1997; Seljak & Zaldarriaga 1997; Ishino et al. 2016), but between the CMB polarization measurements and pulsar timing, which is sensitive to frequencies $\sim 10^{-9}\text{--}10^{-7}$ Hz (e.g., Arzoumanian et al. 2016), are ~ 7 orders of magnitude in frequency space. Proper motion measurements can approach gravitational wave detection in a completely independent manner and bridge the frequency gap between the pulsar timing and CMB polarization methods. The frequency range $f \gtrsim 10^{-15}$ Hz can also be probed using the CMB power spectrum because gravitational waves contribute to the radiation density of the universe and can mimic a massless neutrino, modifying the effective number of neutrino species (e.g., Smith et al. 2006).

Previous observational work on astrometric detection of gravitational waves using active galactic nuclei (AGN) using radio interferometry include Gwinn et al. (1997) and Titov et al. (2011). They quote upper limits on the stochastic gravitational wave background — expressed

in terms of the critical cosmological energy density — of $\Omega_{GW} < 0.11 h_{100}^{-2}$ for $f < 2 \times 10^{-9}$ Hz at 95% confidence (Gwinn et al. 1997) and $\Omega_{GW} < 0.0042 h_{100}^{-2}$ for $f < 10^{-9}$ Hz (Titov et al. 2011). However, we cannot reproduce either of these limits based on their quoted quadrupolar fit parameters.

In this paper, we present detailed methods for astrometric measurement of the gravitational wave background including a maximum likelihood method for extracting correlated signals in vector fields with large significant outliers (the uncorrelated “intrinsic” apparent proper motion induced by relativistic jets; Section 2). We use these methods in Sections 3–5 to obtain new stochastic gravitational wave limits from a Very Long Baseline Array (VLBA)¹ astrometric catalog (Truebenbach & Darling 2017) and from this catalog combined with the first *Gaia* data release (Gaia Collaboration et al. 2016a,b). We also use a *Gaia*-WISE catalog (Paine et al. 2018) to make predictions for the gravitational wave detection sensitivity of *Gaia* by the end of its mission (Section 6).

The only cosmological assumption used for the gravitational wave results is $H_0 = 70 \text{ km s}^{-1} \text{ Mpc}^{-1}$. When expressed as an angular frequency, the Hubble constant becomes $H_0 = 15 \mu\text{as yr}^{-1}$. For superluminal motion² calculations, we additionally assume a flat cosmology with $\Omega_M = 0.27$, and $\Omega_\Lambda = 0.73$.

2. METHODS

To characterize a vector field on a sphere, one can extend the usual spherical harmonic characterization of a scalar field on a sphere to vector spherical harmonics (e.g., Thorne 1980), defined as the gradient and curl of the scalar spherical harmonics, which resemble electric (E) and magnetic (B) fields (Mignard & Klioner 2012):

$$\vec{S}_{\ell m}(\alpha, \delta) = \frac{1}{\sqrt{\ell(\ell+1)}} \vec{\nabla} Y_{\ell m}(\alpha, \delta), \quad (2)$$

and

$$\vec{T}_{\ell m}(\alpha, \delta) = \frac{-1}{\sqrt{\ell(\ell+1)}} \hat{n} \times \vec{\nabla} Y_{\ell m}(\alpha, \delta), \quad (3)$$

where the $\vec{S}_{\ell m}$ is the “spheroidal” E-mode of degree ℓ and order m , $\vec{T}_{\ell m}$ is the “toroidal” B-mode, and \hat{n} is the radial unit vector. $\vec{S}_{\ell m}$, $\vec{T}_{\ell m}$, and \hat{n} are mutually orthogonal, by construction. A general vector field $\vec{V}(\alpha, \delta)$ on the surface of a sphere can be expanded in terms of

¹ The National Radio Astronomy Observatory is a facility of the National Science Foundation operated under cooperative agreement by Associated Universities, Inc.

² See Cohen et al. (1977); Blandford et al. (1977).

this vector spherical harmonic basis using complex coefficients $s_{\ell m}$ and $t_{\ell m}$:

$$\vec{V}(\alpha, \delta) = \sum_{\ell=1}^{\infty} \sum_{m=-\ell}^{\ell} (s_{\ell m} \vec{S}_{\ell m}(\alpha, \delta) + t_{\ell m} \vec{T}_{\ell m}(\alpha, \delta)). \quad (4)$$

The first three spherical harmonic degrees relevant to this treatment (E- and B-mode dipole, quadrupole, and octopole) are listed in Tables 4 and 5 and explicitly as equations with coefficients in Appendix A. We follow the Mignard & Klioner (2012) prescriptions for calculating the power in any mode (the quadrature sum of coefficients, modulo factors of 2),

$$P_{\ell} = s_{\ell 0}^2 + t_{\ell 0}^2 + 2 \sum_{m=1}^{\ell} ((s_{\ell m}^{Re})^2 + (s_{\ell m}^{Im})^2 + (t_{\ell m}^{Re})^2 + (t_{\ell m}^{Im})^2), \quad (5)$$

and use the Z -score to assess significance (Mignard & Klioner 2012, Eqn. 85).

The Gwinn et al. (1997) power (sum of squared “moduli” [amplitudes]) is equivalent to the Mignard & Klioner (2012) power prescription, despite slightly different definitions. One can therefore use the quadrupole power ($\ell = 2$) as described in Equation 5 to obtain an estimate of the gravitational wave energy density:

$$\Omega_{\text{GW}} = \frac{6}{5} \frac{1}{4\pi} \frac{P_2}{H_{\odot}^2} = 0.00042 \frac{P_2}{(1 \mu\text{as yr}^{-1})^2} h_{70}^{-2} \quad (6)$$

The factor of 6/5 in this expression corrects for the 5/6 contribution of the quadrupole to the total gravitational wave signal (Gwinn et al. 1997; Book & Flanagan 2011).

In general, a proper motion catalog that produces a limit on the quadrupole vector spherical harmonics can also provide a similar limit on the octopole (and higher orders), but the expected relative weighting on quadrupole power versus higher multipoles in a stochastic gravitational wave signal declines rapidly, as $\ell^{-4.9}$ (Book & Flanagan 2011). A quadrupole-only limit will typically be the most constraining, despite the additional information contained in higher order modes, so a “bandpower” approach such as that used in CMB signal detection will not be effective (e.g., Bond et al. 1998). We demonstrate this explicitly using data in Section 5. Figure 1 compares an $\ell = 2$ proper motion stream plot to a $(5/6)^{1/2} \vec{V}_2 + (7/60)^{1/2} \vec{V}_3$ vector field. The quadrupole and octopole coefficients were randomly selected from normal distributions with the appropriate $\sqrt{2}$ scaling of the $m = 0$ terms. The differences between the two cases are subtle because the octopole power is de-weighted by a factor of ~ 7 compared to the quadrupole.

3. DATA SOURCES AND PROPER MOTIONS

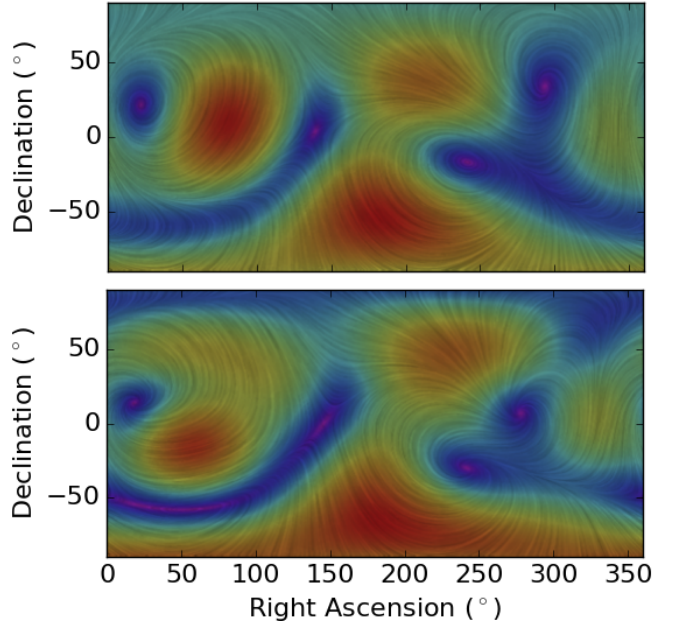


Figure 1. Randomly generated all-sky quadrupole (top) and quadrupole plus octopole (bottom) E- and B-mode stream plots in equatorial coordinates (see Section 2). For the combined quadrupole and octopole plot, the weighting is $(5/6)^{1/2}$ and $(7/60)^{1/2}$, respectively, which accounts for 95% of the expected signal power (the remainder is in higher multipole modes; Book & Flanagan 2011). Streamlines indicate the vector field direction, and the colors indicate the vector amplitude, from violet (zero) to red (maximum).

We measure proper motions from astrometric time series using VLBA data only and VLBA data combined with a single *Gaia* epoch. For both time series, we fit position versus time in right ascension and declination separately using error-weighted linear least-squares bootstrapped to incorporate the effect of outlier epochs, as described in Truebenbach & Darling (2017).

3.1. VLBA Catalog

The VLBA astrometric catalog is described and characterized in detail in Truebenbach & Darling (2017). In summary, the catalog contains 713 objects with mean astrometric uncertainties of $24 \mu\text{as yr}^{-1}$. These were obtained from long-term astrometric monitoring programs as well as new observations. Proper motions were measured from astrometric time series using a bootstrapped error-weighted least-squares fit for each object in each coordinate, substantially improving on previous proper motion measurements for most objects.

The time baselines spanned by the new and archival data cover the range 6.4 yr to 27.2 yr (1.2×10^{-9} Hz to 5.0×10^{-9} Hz). The median time series spans 22.2 yr, which is equivalent to $f = 1.4 \times 10^{-9}$ Hz. Figure 2 shows the distribution of observed frequencies for the

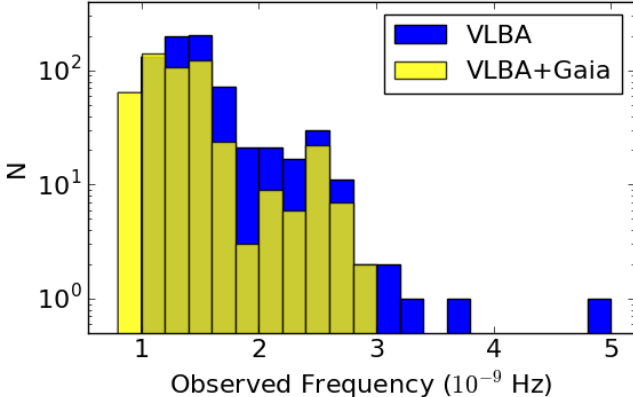


Figure 2. Distribution of observed frequencies obtained from astrometric time series of the VLBA and VLBA+*Gaia* catalogs. The upper bound on the gravitational wave frequency sensitivity of an object is the inverse of the time span used to measure its proper motion. The gravitational wave frequencies probed by these proper motions span the range $6 \times 10^{-18} \text{ Hz} \lesssim f \lesssim 1 \times 10^{-9} \text{ Hz}$ (see Section 3.1).

catalog. The majority (95%) of objects sample the range $f_{obs} = 1.0\text{--}2.5 \times 10^{-9} \text{ Hz}$. The lower bound on detectable frequencies is set by the distance of the catalog objects, which must be greater than the wavelength of the gravitational waves. The sensitivity of the sample to the longest wavelength gravitational waves will therefore be a function of frequency because the sample size decreases with distance. The median redshift is 1.10, and the upper and lower quartile divisions are 0.594 and 1.64. We conservatively set the lower bound on frequency using the first redshift quartile, $z_{25\%} = 0.594$, where 75% of the sample can still be used to detect gravitational waves. Using our assumed cosmology, the light travel time is 5.74 Gyr, which corresponds to $6 \times 10^{-18} \text{ Hz}$. The astrometry is therefore sensitive to gravitational waves with $6 \times 10^{-18} \text{ Hz} \lesssim f \lesssim 1 \times 10^{-9} \text{ Hz}$.

While this catalog shows very low proper motion errors, the proper motions themselves can be substantial and significant due to relativistic radio jet motion (see Section 3.2). This “intrinsic” proper motion is uncorrelated between objects, but introduces special challenges to detecting small-amplitude correlated global proper motions. Section 4 presents a solution to this uncorrelated large-amplitude significant-signal contamination problem.

3.2. VLBA+*Gaia* Catalog

The first *Gaia* data release (DR1) catalog (Gaia Collaboration et al. 2016a) contains a single-epoch (2015.0) position for 2191 AGN in the International Celestial Reference Frame (ICRF2) catalog (Mignard et al. 2016). 577 of these are VLBA sources in the Truebenbach &

Darling (2017) catalog, and we use them to measure proper motions from the VLBA-*Gaia* time series. Median uncertainties in the *Gaia* astrometry of these objects are 518 μas and 459 μas in right ascension and declination, respectively.

To create a VLBA+*Gaia* proper motion catalog, we perform a 500-iteration bootstrap error-weighted least-squares fit to the VLBA time series as described by Truebenbach & Darling (2017), but we include the *Gaia* point in every fit rather than allowing it to fall into the bootstrap selection pool. This causes the *Gaia* point to act as a loose astrometric anchor, to within its uncertainty. When there are many radio epochs in a time series, the *Gaia* point will still have a minor impact on the best-fit proper motion.

We assess the *Gaia* offset from the VLBA-only proper motion prediction for the *Gaia* epoch strictly based on the uncertainty in the *Gaia* measurement, which is typically larger than the prediction uncertainty of the time series fit. The proper motions obtained from the time series that include a single *Gaia* epoch are typically not significantly altered from the VLBA-only results, but there are some notable exceptions. It is remarkable that 88% of the objects’ proper motions show consistency between the radio trend and the *Gaia* position. In most of these cases (87% of the consistent subset), the measured proper motion, given its uncertainty, is consistent with zero, which implies that the optical and radio positions coincide with no motion to within the measurement uncertainty.

In 13% of the sample, the *Gaia* epoch extends the time series beyond the VLBA epochs, agrees with the VLBA proper motion, and generally improves the proper motion solution (see 0007+171 in Figure 3). We assume in these cases that the optical and radio centroids are coincident (as is the case with most objects in the sample).

In 12% of the sample, the *Gaia* epoch is significantly ($> 3\sigma$) offset from the VLBA proper motion fit in one or both coordinates, indicating that the optical and radio centroids do not coincide. Figure 3 shows an example, 0003+380, where the *Gaia* astrometry is significantly offset in both coordinates. We cannot yet say whether the radio and optical proper motions differ because there is only one optical astrometric epoch. There are many possible reasons for radio-optical offsets, including optically faint jet emission, optical light from the host galaxy, dust obscuration of the AGN, and offset radio and optical emission regions within jets (e.g., Kovalev et al. 2016). Given these scenarios, it is surprising that 88% of the sample does show good radio-optical coincidence at the sub-mas level (but see Petrov & Kovalev 2017).

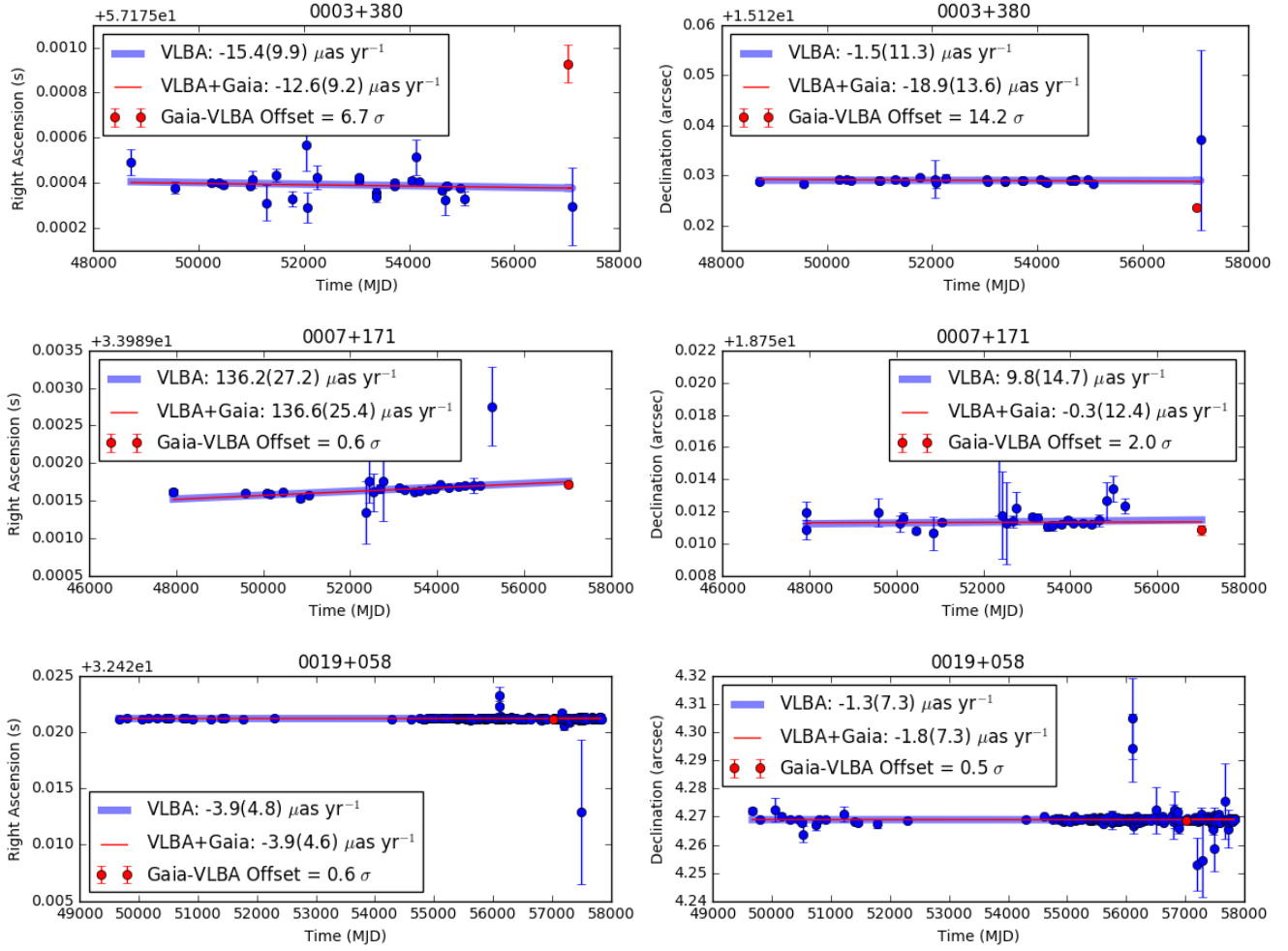


Figure 3. Example time series astrometric fits of VLBA only (blue) and VLBA plus the 2015.0 *Gaia* epoch (red). The columns depict the Right Ascension (left) and the Declination (right), and the proper motions and their errors are indicated in the inset boxes. Top: 0003+380 shows significant *Gaia*-VLBA inconsistency, indicating physical offsets between the radio and optical emission regions. Middle: 0007+171 shows highly significant (and superluminal) motion where the optical and radio emission regions are consistent. This is also an example of the *Gaia* epoch substantially extending the time series. Bottom: 0019+058 shows agreement between the VLBA and *Gaia* astrometry where no proper motion is detected. This case represents the majority (77%) of the astrometric sample.

In 9% of the subsample with good VLBA+*Gaia* agreement (8% of the total sample) the proper motion is significant ($> 5\sigma$ in at least one coordinate) and intrinsic to the object (not cosmological, caused by gravitational waves, or observer-induced). For example, 0007+171 shows a right ascension proper motion of $136.6(25.4) \mu\text{as yr}^{-1}$ (Figure 3 and Tables 6 and 7). At a redshift of $z = 1.601$ (Wills & Wills 1976), this proper motion coincides with apparent superluminal motion of $10.1(1.9)c$ in the object’s rest frame.

Apparent velocities are calculated in the source rest frame using the proper motion distance D_M , which is equal to the line-of-sight comoving distance in a flat cosmology and related to the angular diameter distance D_A as $D_M = D_A(1+z)$ (Hogg 1999). The redshift scale factor translates the observer-frame time interval

used to calculate apparent velocity into the object rest-frame time interval. We therefore calculate the apparent transverse velocity from proper motion via

$$\vec{v} = \vec{\mu} D_M \quad (7)$$

where D_M may be expressed in distance per radian or most often kpc arcsec $^{-1}$.

In total, there are 22 objects that show superluminal optical and radio motion, up to $10.1 c$. Table 6 lists the properties of these objects. We interpret these observations to indicate that the AGN radio jets also show significant detectable optical emission, even at substantial redshifts. It is noteworthy that optical superluminal motion has only been observed in the local universe in a small number of objects including M87 and 3C264 (e.g., Biretta et al. 1999; Meyer et al. 2015).

Table 7 lists the VLBA-only and the VLBA+*Gaia* proper motions as well as the *Gaia* offsets from the VLBA-only fits. For signal extraction from this catalog, we exclude objects with significant (3σ) *Gaia* offsets in either coordinate direction. After culling, 508 objects remain in this sample, and these are used in the vector spherical harmonic fits (Sections 4 and 5).

The time baselines spanned by the VLBA+*Gaia* proper motion catalog are somewhat longer than the VLBA-only catalog (see Figure 2). Time series range from 10.6 yr to 37.6 yr (8.4×10^{-10} Hz to 3.0×10^{-9} Hz), and the median time series spans 24.9 yr, which is equivalent to $f = 1.3 \times 10^{-9}$ Hz. The majority (95%) of objects sample the range $f_{obs} = 0.8\text{--}2.5 \times 10^{-9}$ Hz. The median redshift is 1.23, and the upper and lower quartile divisions are 0.73 and 1.80. The first redshift quartile, $z_{25\%} = 0.73$, with light travel time 6.55 Gyr, sets the lower bound on frequency of 5×10^{-18} Hz. The $\ell \geq 2$ correlated proper motions used to constrain the stochastic gravitational wave background are therefore sensitive to waves with frequencies 5×10^{-18} Hz $\lesssim f \lesssim 0.8 \times 10^{-9}$ Hz.

3.3. *Gaia Catalog*

The advantages of extragalactic *Gaia* proper motions over radio interferometric proper motions lie in the factor of ~ 1000 increase in number of optical sources over radio and the (generally) lower intrinsic optical proper motions. These advantages may overcome the less precise astrometry and shorter time baseline of *Gaia* compared to geodetic VLBI monitoring (in the short term).

The *Gaia* DR1 catalog contains a single epoch position for AGN, but the expected end-of-mission proper motion uncertainties can be used to predict the sensitivity of the final *Gaia* catalog to gravitational waves. To first order, the vector proper motion error of each object depends on its ecliptic angle and optical *G*-band magnitude³. We use the pyGaia⁴ package to predict the proper motion errors for each object in the 567,721 AGN Paine et al. (2018) WISE-*Gaia* sample. Paine et al. (2018) present the expected uncertainties, the sky distribution, and the potential systematics of the sample. We use this catalog in Section 6 to predict the expected *Gaia* end-of-mission sensitivity to the stochastic gravitational wave background.

4. SIGNAL EXTRACTION

The challenge to vector spherical harmonic fitting posed by radio sources is their often significant large

apparent intrinsic proper motions induced by relativistic jets. These intrinsic proper motions are uncorrelated between objects, but can dominate an error-weighted least-squares fit of the correlated proper motions. Investigators measuring the secular aberration drift dipole have therefore heavily censored their samples in order to maximize the signal of interest (e.g., Titov et al. 2011; Titov & Lambert 2013), but this requires *a priori* knowledge of the expected signal. A different approach can be bootstrap resampling, which was successfully implemented by Truebenbach & Darling (2017) to extract the secular aberration drift dipole induced by the barycenter acceleration about the Galactic Center with minimal data clipping.

Here we implement a maximum likelihood MCMC “permissive fit” method that allows for highly significant large-departure data points by assuming that the mismatch between model and data will in some cases be bounded from below by the measured uncertainty (Sivia & Skilling 2006, p. 168). This method, rather than minimizing an error-weighted data-model residual $R_i = (D_i - \text{Model})/\sigma_i$ for each data point D_i with uncertainty σ_i , maximizes the logarithm of the posterior probability density function

$$L = \text{constant} + \sum_{i=1}^N \ln \left(\frac{1 - e^{-R_i^2/2}}{R_i^2} \right). \quad (8)$$

In this work, the data are the positions and proper motions of extragalactic objects, the model is a linear combination of vector spherical harmonics evaluated at each object position, and the uncertainties are the proper motion errors (uncertainties in the positions of objects have no impact on low- ℓ signals). To assess the model fits and uncertainties, we employ a MCMC technique using lmfit (Newville et al. 2014) to obtain the maximum likelihood and confidence intervals for each fit parameter directly from the resulting distribution of outcomes.

For the vector spherical harmonic fits, all coefficients and uncertainties are maximum likelihood estimates. The power in a given mode is calculated from Equation 5, and its significance is estimated using a Z -score following Mignard & Klioner (2012), Eqn. 85.

4.1. *The Secular Aberration Drift Dipole*

We start with a fit of the E- and B-mode dipole signals in both catalogs, which must be removed from vector fields before attempting to measure higher order modes. While the vector spherical harmonics are in principle orthonormal, there can be correlation between degrees and orders when fitting the harmonics to discrete sparsely sampled non-uniform noisy data, so “nuisance” signals must be subtracted. We simultaneously fit for

³ <https://www.cosmos.esa.int/web/gaia/science-performance>

⁴ <https://pypi.python.org/pypi/PyGaia>

both E- and B-mode dipoles (aberration drift and rotation, respectively) to capture any residual signature of a non-inertial frame (or other cosmic rotation) as well as any correlations between the two modes (even if the B-mode dipole is non-significant, there can still be crosstalk with the E-mode dipole). Following Mignard & Klioner (2012), the dipole equations are listed in Tables 4 and 5 and explicitly as equations with coefficients in Appendix A.

Table 1 lists the dipole fit coefficients for the VLBA and VLBA+*Gaia* samples. We significantly detect the secular aberration drift with 5.5σ and 5.1σ significance, respectively. The E-mode dipole apex lies at $279^\circ 2(9.8)$, $-27^\circ 0(8.7)$ and $274^\circ 0(9.3)$, $-18^\circ 0(9.2)$, and is consistent with the Galactic Center ($266^\circ 4$, $-29^\circ 0$) in each case (Figure 4). The dipole amplitude is $1.70(0.26)$ and $1.70(0.29)$ $\mu\text{as yr}^{-1}$, which is substantially smaller than expected. For example, Titov & Lambert (2013) find $6.4(1.1)$ $\mu\text{as yr}^{-1}$, and Xu et al. (2013) obtain $5.8(0.3)$ $\mu\text{as yr}^{-1}$. These are consistent with the expectation of $5.5(0.2)$ $\mu\text{as yr}^{-1}$ based on barycenter orbital parameters obtained from Galactic maser parallaxes and proper motions and the Sgr A* reflex motion (Reid et al. 2014). The amplitude of the dipole measured here is likely suppressed by the no-net-rotation constraint imposed by the global fitting used to produce the ICRF catalog (see Truebenbach & Darling (2017) for a detailed discussion). For the purposes of detecting higher multipole modes in the proper motion data, we simply need to measure whatever dipole is present and subtract the dipole fit from each proper motion catalog before fitting higher multipoles to extract (or constrain) the gravitational wave signal.

No rotation is detected: the B-mode dipole fits are not significant (1.2σ or less), with square root power of $1.89(0.74)$ $\mu\text{as yr}^{-1}$ for the VLBA catalog and $1.29(0.79)$ $\mu\text{as yr}^{-1}$ for VLBA+*Gaia*. These correspond to angular rotation rates of $0.65(0.26)$ and $0.45(0.27)$ $\mu\text{as yr}^{-1}$, respectively.

4.2. Gravitational Waves

For each catalog, we simultaneously fit E- and B-mode quadrupolar vector spherical harmonics for the best constraint on the stochastic gravitational wave background. We also simultaneously fit E- and B-mode quadrupole and octopole coefficients, but this fit is less constraining than quadrupole alone, as described in Section 2 and demonstrated explicitly in Section 5. Measuring the quadrupole and octopole powers separately is a way to test the isotropy of the background, which is assumed when combining the two modes to obtain a limit on Ω_{GW} . The quadrupole and octopole vector spherical

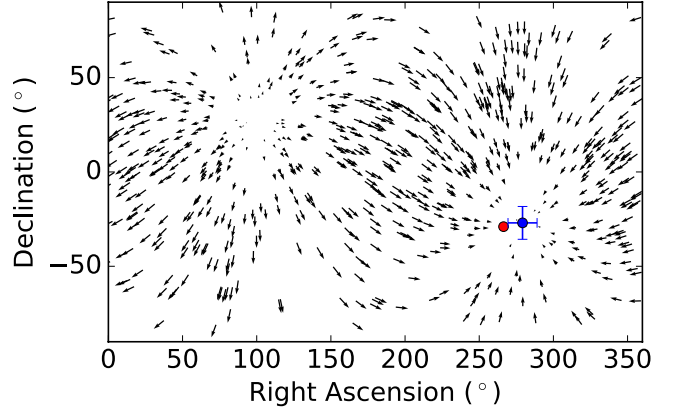


Figure 4. Maximum likelihood secular aberration drift (E-mode dipole) model fit to the VLBA sample plotted in equatorial coordinates. The fit parameters and uncertainties are listed in Table 1. The red circle indicates the Galactic Center, and the point with the error bars shows the dipole apex obtained from the dipole (simultaneous E- and B-mode) fit.

Table 1. Dipole Fits

	VLBA	VLBA+ <i>Gaia</i>
Quantity	Amplitude ($\mu\text{as yr}^{-1}$)	Amplitude ($\mu\text{as yr}^{-1}$)
E-Mode Dipole (Aberration Drift)		
s_{10}	$-2.24(0.74)$	$-1.52(0.78)$
s_{11}^{Re}	$-0.50(0.53)$	$-0.21(0.53)$
s_{11}^{Im}	$-3.07(0.54)$	$-3.29(0.61)$
$\sqrt{\mathbf{P}_1^s}$	$4.93(0.76)$	$4.91(0.85)$
Z-score ^a	5.5	5.1
B-Mode Dipole (Rotation)		
t_{10}	$-0.72(0.62)$	$-0.51(0.68)$
t_{11}^{Re}	$+1.17(0.52)$	$0.76(0.55)$
t_{11}^{Im}	$-0.40(0.66)$	$-0.36(0.68)$
$\sqrt{\mathbf{P}_1^t}$	$1.89(0.74)$	$1.29(0.79)$
Z-score ^a	1.2	0.1

^aThis statistic is unitless.

NOTE—Fits are simultaneously made to electric and magnetic dipole vector fields.

harmonics are listed in Tables 4 and 5 and explicitly as equations with coefficients in Appendix A, Equations A3–A6.

It is incorrect to obtain a limit on Ω_{GW} from the parameters of a non-significant quadrupole fit to a vector field. When no significant signal is detected, we follow the method described by Gwinn et al. (1997): assuming independent Gaussian errors on the fit coefficients

as determined using the above methods, we resample the fit components and recalculate the quadrupole power 10,000 times. We set the upper limit to be 95th percentile of the quadrupole power distribution. This method gives a less-constraining result than has been quoted in previous work, such as Titov et al. (2011).

A stochastic gravitational wave background (or a reliable limit) should show equal power in the E- and B-modes (Book & Flanagan 2011). One can therefore identify spurious, non-gravitational wave signals by comparing the power in the two modes.

5. RESULTS

5.1. VLBA

We fit the vector spherical harmonic quadrupole to the Truebenbach & Darling (2017) VLBA proper motion catalog with minimal restrictions on the fit sample. We omit two objects with proper motion amplitudes greater than 1 milliarcsec yr⁻¹, leaving 711 objects in the catalog. After E-mode dipole subtraction, a simultaneous E- and B-mode quadrupole fit produced no significant signal, with a total quadrupole power of $\sqrt{P_2} = 1.83(0.72)$ $\mu\text{as yr}^{-1}$. Table 2 shows the fit components, mutually consistent (and non-significant) E- and B-mode powers ($\sqrt{P_2^s} = 1.46(0.69)$ $\mu\text{as yr}^{-1}$ and $\sqrt{P_2^t} = 1.11(0.77)$ $\mu\text{as yr}^{-1}$, respectively), and the Z-score of the fit. Using the resampling method described above (Section 4.2), we obtain a 95% confidence limit on the stochastic gravitational wave energy density of $\Omega_{GW} < 0.0064$ (see Equation 6). Direct conversion of the non-significant quadrupolar power to energy density gives a smaller (non-significant) value: $\Omega_{GW} = 0.0014(0.0011)$. This is roughly equivalent to a dimensionless gravitational wave strain amplitude of $h \simeq 10^{-10}$ for $f \simeq 10^{-9}$ Hz ($h \sim (H_0/f)\sqrt{\Omega_{GW}}$; Book & Flanagan 2011). The maximum proper motion amplitude in the quadrupole is 1.0 $\mu\text{as yr}^{-1}$, which is equivalent to $h \simeq 10^{-10}$ for $f \simeq 10^{-9}$ Hz ($h \sim \mu/f$).

A simultaneous quadrupole and octopole fit in both E- and B-modes produces a weaker constraint on the stochastic gravitational wave background, as expected (see Section 2): $\sqrt{P_2} = 3.53(1.09)$ $\mu\text{as yr}^{-1}$, $\sqrt{P_3} = 4.98(0.92)$ $\mu\text{as yr}^{-1}$, and $\Omega_{GW} < 0.032$ (95% confidence limit). To calculate the above limit on Ω_{GW} from the non-significant quadrupole and octopole fits, we substitute a weighted power into Equation 6, $1.05(P_2 + P_3)$ in the place of $(6/5)P_2$, and resample the fit coefficients to find a 95% confidence limit. Table 3 lists the coefficients, mode powers, and Z-scores for this fit.

5.2. VLBA+Gaia

Table 2. Quadrupole Fits

Quantity	VLBA	VLBA+ <i>Gaia</i>
	Amplitude ($\mu\text{as yr}^{-1}$)	Amplitude ($\mu\text{as yr}^{-1}$)
Quadrupole		
s_{20}	0.83(0.72)	1.72(0.78)
s_{21}^{Re}	0.80(0.47)	1.16(0.52)
s_{21}^{Im}	-0.22(0.48)	-0.49(0.51)
s_{22}^{Re}	-0.17(0.58)	-0.04(0.59)
s_{22}^{Im}	0.06(0.44)	0.74(0.46)
$\sqrt{P_2^s}$	1.46(0.69)	2.70(0.74)
t_{20}	-0.48(0.66)	-1.17(0.70)
t_{21}^{Re}	0.01(0.50)	-0.68(0.58)
t_{21}^{Im}	-0.16(0.43)	-0.41(0.47)
t_{22}^{Re}	0.43(0.53)	0.25(0.56)
t_{22}^{Im}	0.54(0.60)	0.81(0.60)
$\sqrt{P_2^t}$	1.11(0.77)	2.01(0.78)
$\sqrt{P_2}$	1.83(0.72)	3.36(0.75)
Z-score ^a	-0.7	1.9

^aThis statistic is unitless.

NOTE—Fits are simultaneously made to electric and magnetic quadrupole vector fields. Parenthetical quantities indicate 1σ uncertainties.

We subtract the E-mode dipole and then fit the vector spherical harmonic quadrupole to the 508-object VLBA+*Gaia* proper motion catalog with no proper motion restrictions. The simultaneous E- and B-mode quadrupole fit is not significant; the total quadrupole power is $\sqrt{P_2} = 3.36(0.75)$ $\mu\text{as yr}^{-1}$, and the E- and B-mode powers are consistent: $\sqrt{P_2^s} = 2.70(0.74)$ $\mu\text{as yr}^{-1}$ and $\sqrt{P_2^t} = 2.01(0.78)$ $\mu\text{as yr}^{-1}$, respectively. Table 2 lists the fit components and the Z-score of the fit. The 95% confidence limit on the stochastic gravitational wave energy density is $\Omega_{GW} < 0.011$ (see Equation 6).

The simultaneous quadrupole and octopole fit in both E- and B-modes yields $\sqrt{P_2} = 3.23(1.01)$ $\mu\text{as yr}^{-1}$, $\sqrt{P_3} = 5.10(0.89)$ $\mu\text{as yr}^{-1}$, and $\Omega_{GW} < 0.028$ (95% confidence limit). This limit on the stochastic gravitational wave background is less constraining than the quadrupole-only fit, as expected, but is slightly more constraining than the VLBA-only quadrupole plus octopole fit. Table 3 lists the coefficients, mode powers, and Z-scores for this fit.

6. GAIA PREDICTIONS

The rough expectation for a stochastic gravitational wave background limit obtained from *Gaia* presented by

Table 3. Quadrupole and Octopole Fits

	VLBA	VLBA+ <i>Gaia</i>
Quantity	Amplitude	Amplitude
	(μas yr ⁻¹)	(μas yr ⁻¹)
Quadrupole		
s_{20}	0.55(0.98)	0.58(0.70)
s_{21}^{Re}	0.88(0.62)	0.29(0.71)
s_{21}^{Im}	-0.30(0.52)	-0.99(0.61)
s_{22}^{Re}	-0.28(0.69)	-0.42(0.76)
s_{22}^{Im}	0.04(0.30)	0.05(0.54)
t_{20}	-0.27(0.20)	-0.18(0.53)
t_{21}^{Re}	0.78(0.63)	-0.10(0.57)
t_{21}^{Im}	0.13(0.36)	-1.01(0.48)
t_{22}^{Re}	-0.50(0.37)	0.02(0.01)
t_{22}^{Im}	2.05(0.84)	1.66(0.83)
$\sqrt{P_2}$	3.53(1.09)	3.23(1.01)
Z-score ^a	1.9	1.2
Octopole		
s_{30}	-0.75(0.87)	-0.34(1.02)
s_{31}^{Re}	-0.35(0.18)	0.42(0.53)
s_{31}^{Im}	0.00(0.24)	0.82(0.73)
s_{32}^{Re}	1.57(0.66)	1.10(0.66)
s_{32}^{Im}	0.59(0.61)	0.61(0.51)
s_{33}^{Re}	0.60(0.53)	-0.37(0.52)
s_{33}^{Im}	0.85(0.58)	0.39(0.58)
t_{30}	-0.10(0.81)	-0.41(0.96)
t_{31}^{Re}	-1.43(0.58)	-2.68(0.62)
t_{31}^{Im}	0.78(0.53)	0.94(0.57)
t_{32}^{Re}	0.90(0.59)	0.86(0.60)
t_{32}^{Im}	-0.77(0.49)	-0.04(0.73)
t_{33}^{Re}	-2.01(0.75)	-0.73(0.84)
t_{33}^{Im}	-0.12(0.61)	-0.90(0.57)
$\sqrt{P_3}$	4.98(0.92)	5.10(0.89)
Z-score ^a	3.4	2.6

^aThis statistic is unitless.

NOTE—Fits are simultaneously made to electric and magnetic quadrupole and octopole vector fields. Parenthetical quantities indicate 1σ uncertainties.

Book & Flanagan (2011) was $\Omega_{GW} \lesssim 10^{-6}$ for $f \lesssim 10^{-8}$ Hz, but this was under the assumption of a proper motion uncertainty of $\sigma_\mu = 10 \text{ } \mu\text{as yr}^{-1}$ per source and using 10^6 objects. The revised end-of-mission error budgets, which have the largest impact on faint sources, have $\sigma_\mu \sim 200 \text{ } \mu\text{as yr}^{-1}$ per quasar, and $\sim 5 \times 10^5$ objects (Paine et al. 2018), so we expect $\Omega_{GW} \lesssim 10^{-3}$.

To confirm this expectation, we use the expected end-of-mission proper motion errors on the extragalactic

Gaia-WISE catalog compiled by Paine et al. (2018) and described in Section 3.3. We randomly sample vector proper motions from within the predicted error budget for each object assuming Gaussian errors. Provided that the barycenter acceleration about the Galactic Center can be removed from the data, the resulting proper motions should be uncorrelated and represent a no-signal noisy dataset that can be used to predict the best possible limit on a gravitational wave signal. Unlike the *Gaia* Universe model snapshot (GUMS) sample (Robin et al. 2012), this catalog represents real objects detected in *Gaia* that will likely be employed when final proper motions are measured.

After randomly sampling from within the proper motion error budgets for each object, we performed an error-weighted least-squares fit of 500 randomly generated E- and B-mode quadrupolar gravitational wave signals with the quadrupolar power in the range $0.5 \text{ } \mu\text{as yr}^{-1} \leq \sqrt{P_2} \leq 5 \text{ } \mu\text{as yr}^{-1}$ in 25 logarithmic steps with 20 trials each. For each trial, we add the input proper motion quadrupolar signal to the catalog proper motions and then fit simultaneous E- and B-mode quadrupole vector spherical harmonics (listed in Appendix A) to obtain a fit power. For each input power, we calculate the mean and standard deviation of the best-fit power to assess the offset and scatter of the fit compared to the input.

Figure 5 shows the results of these fit trials, recast in terms of Ω_{GW} . For $\Omega_{GW} \gtrsim 10^{-3}$, we reliably recover the input gravitational wave signal with some scatter, but a clear noise floor arises for $\Omega_{GW} \lesssim 6 \times 10^{-4}$ such that the (non-significant) fit does not fall below $\Omega_{GW} \sim 6 \times 10^{-4}$. This is the limit on the stochastic gravitational wave background that *Gaia* may achieve using the Paine et al. (2018) *Gaia*-WISE extragalactic proper motion catalog, which agrees with the rough expectation above.

7. DISCUSSION

The VLBA+*Gaia* fits are less constraining on the stochastic gravitational wave background than the VLBA-only fits, despite the generally improved proper motion solutions obtained from the VLBA+*Gaia* time series. Since Ω_{GW} depends on the vector spherical harmonic mode power, it will scale roughly as N , not \sqrt{N} , and the reduced VLBA+*Gaia* sample size should decrease sensitivity by a factor of roughly $\sqrt{2}$ compared to the VLBA-only sample. The sample size accounts for some, but not all, of the difference in limits on Ω_{GW} .

The expected *Gaia* proper motions, despite the substantially lower precision compared to radio-based astrometry, will further constrain the stochastic gravitational wave background by roughly an order of magni-

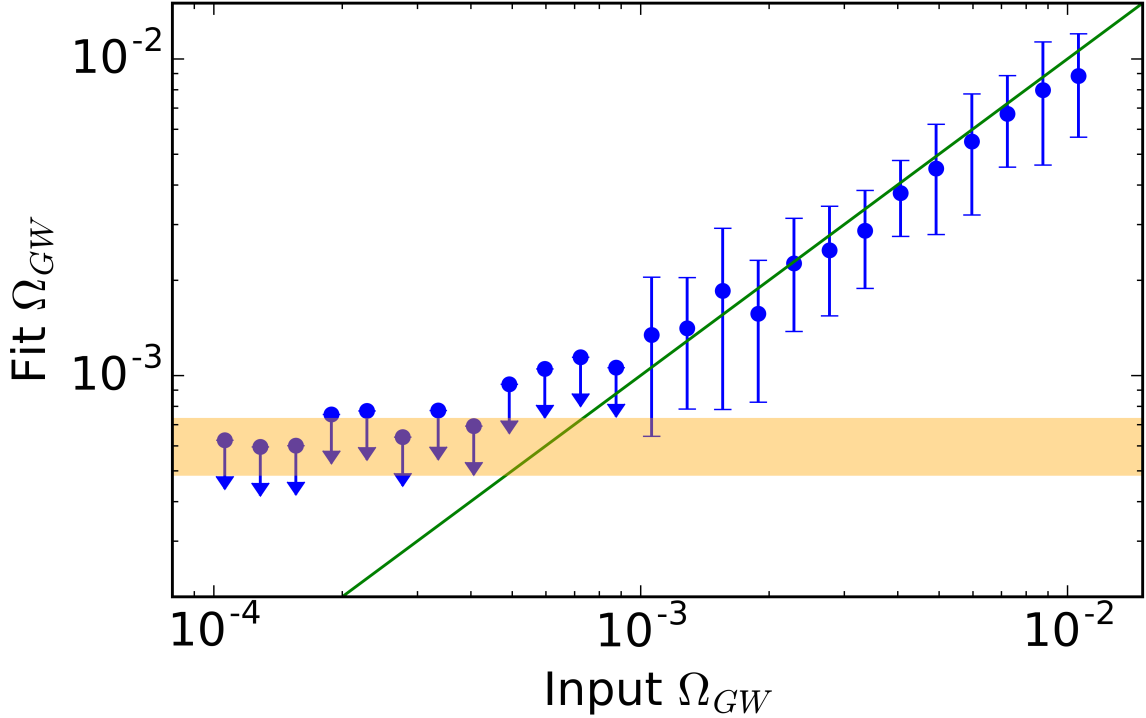


Figure 5. Fit vs. input values for the stochastic gravitational wave background energy density, Ω_{GW} , expected from *Gaia* proper motions. Points and their error bars indicate the mean and standard deviation of 20 recovery trials per random injected signal. Arrows indicate non-significant fits. The green line indicates the one-to-one perfect signal recovery locus, and the orange bar shows the $\Omega_{GW} = 6 \times 10^{-4}$ noise floor imposed by the end-of-mission *Gaia* proper motion sensitivity to AGN in the *Gaia*-WISE catalog.

tude due to the larger extragalactic sample size available in visible light. The *Gaia* proper motions are also expected to be less dominated by the intrinsic proper motions caused by relativistic AGN jets. While the VLBA+*Gaia* sample identified 22 new cases of radio and optical superluminal motion and 23 cases of sub-luminal significant intrinsic proper motion (8% of the 577-object sample in total), these are radio-selected objects. The Paine et al. (2018) *Gaia*-WISE sample is optical- and infrared-selected and will therefore not be so jet-dominated as a VLBI radio-selected sample, and it is therefore reasonable to assume that the vast majority of *Gaia* objects will show no detectable intrinsic proper motion.

The astrometric gravitational wave limit may be improved by increasing the sample size in either radio or visible light. Identifying additional AGN in the *Gaia* catalog may decrease the expected Ω_{GW} noise floor by at most a factor of 2 if one can achieve a 10^6 -object sample. In this case, one might achieve $\Omega_{GW} \lesssim 2 \times 10^{-4}$, which is nonetheless substantially larger than the $\sim 10^{-6}$ value predicted by Book & Flanagan (2011). Improvements could also arise from an extended *Gaia* mission or better-than-expected performance of the main mission. Enhancing the radio sample size is a possibility, perhaps

by an order of magnitude. Assuming similar astrometric precision and intrinsic proper motions to the current catalog, this would reduce the 95% confidence limit to $\Omega_{GW} \lesssim 6 \times 10^{-4}$, which is similar to the *Gaia* limit.

8. CONCLUSIONS

We have obtained limits on the low-frequency stochastic gravitational wave background using VLBA astrometry alone and VLBA astrometry combined with the first *Gaia* epoch. We demonstrate that a quadrupole signal is the most constraining and obtain 95% confidence limits on the gravitational wave energy density of $\Omega_{GW} < 0.0064$ over the frequency range 6×10^{-18} Hz $\lesssim f \lesssim 1 \times 10^{-9}$ Hz for the VLBA proper motions. When *Gaia* is included proper motion errors improve, but the limit is less constraining, mainly due to a reduced sample size: $\Omega_{GW} < 0.011$. The noise threshold for the VLBA fit is roughly equivalent to a dimensionless gravitational wave strain amplitude of $h \simeq 10^{-10}$ for $f \simeq 10^{-9}$ Hz.

We also predict the limit that may be obtained with the full *Gaia* data release that includes proper motions (or limits) of AGN. One hurdle is the identification of AGN among the 1000-fold more numerous stars in the *Gaia* catalog and finding an all-sky distribution that is amenable to low- ℓ mode fitting, but provided this can

be done (see Paine et al. 2018), then we predict that *Gaia* will find a noise floor of $\Omega_{GW} \lesssim 6 \times 10^{-4}$ using $\sim 6 \times 10^5$ objects.

Astrometric limits on the stochastic gravitational wave background will continue to improve with time as geodetic monitoring of radio-loud AGN continues, but substantial improvements will need to come from growing the number of objects monitored. The next post-*Gaia* advance could be made by a Next Generation Very Large Array were it to have substantial collecting area on VLBA baselines (Bower et al. 2015).

We thank David Gordon (NASA Goddard Space Flight Center) for making much of this work possible and Mark Reid (Smithsonian Astrophysical Observatory) for helpful discussions. We also thank the anonymous referee for helpful suggestions. The authors acknowledge support from the NSF grant AST-1411605

and the NASA grant 14-ATP14-0086. This work has made use of data from the European Space Agency (ESA) mission *Gaia* (<https://www.cosmos.esa.int/gaia>), processed by the *Gaia* Data Processing and Analysis Consortium (DPAC, <https://www.cosmos.esa.int/web/gaia/dpac/consortium>). Funding for the DPAC has been provided by national institutions, in particular the institutions participating in the *Gaia* Multilateral Agreement. We acknowledge the *Gaia* Project Scientist Support Team and the *Gaia* Data Processing and Analysis Consortium for the pyGaia software. This research has made use of NASA’s Astrophysics Data System Bibliographic Services and the NASA/IPAC Extragalactic Database (NED), which is operated by the Jet Propulsion Laboratory, California Institute of Technology, under contract with the National Aeronautics and Space Administration.

Facilities: Gaia, VLBA

Software: lmfit (Newville et al. 2014), pyGaia

REFERENCES

- Arzoumanian, Z., Brazier, A., Burke-Spolaor, S., et al. 2016, ApJ, 821, 13
- Biretta, J. A., Sparks, W. B., & Macchetto, F. 1999, ApJ, 520, 621
- Blandford, R. D., McKee, C. F., & Rees, M. J. 1977, Nature, 267, 211
- Bond, J. R., Jaffe, A. H., & Knox, L. 1998, Phys. Rev. D, 57, 2117
- Book, L. G. & Flanagan, É. É. 2011, Phys. Rev. D, 83, 024024
- Bower, G. C., Demorest, P., Braatz, J., et al. 2015, ArXiv e-prints, arXiv:1510.06432
- Braginsky, V. B., Kardashev, N. S., Polnarev, A. G., & Novikov, I. D. 1990, Nuovo Cimento B, 105, 1141
- Cohen, M. H., Kellermann, K. I., Shaffer, D. B., et al. 1977, Nature, 268, 405
- Gaia Collaboration, A. G. A. Brown, A. Vallenari, T. Prusti, J. H. J. de Bruijne, F. Mignard, R. Drimmel, C. Babusiaux, C. A. L. Bailer-Jones, U. Bastian, et al. 2016a, A&A, 595, A2
- Gaia Collaboration, T. Prusti, J. H. J. de Bruijne, A. G. A. Brown, A. Vallenari, C. Babusiaux, C. A. L. Bailer-Jones, U. Bastian, M. Biermann, D. W. Evans, et al. 2016b, A&A, 595, A1
- Gwinn, C. R., Eubanks, T. M., Pyne, T., Birkinshaw, M., & Matsakis, D. N. 1997, ApJ, 485, 87
- Hogg, D. W. 1999, astro-ph/9905116
- Ishino, H., Akiba, Y., Arnold, K., et al. 2016, Proc. SPIE, 9904
- Kaiser, N. & Jaffe, A. 1997, ApJ, 484, 545
- Kamionkowski, M., Kosowsky, A., & Stebbins, A. 1997, PhRvL, 78, 2058
- Kovalev, Y. Y., Petrov, L., & Plavin, A. V. 2016, A&A, 598, L1
- Malkin, Z. M. 2016, Astronomy Reports, 60, 996
- Meyer, E. T., Georganopoulos, M., Sparks, W. B., et al. 2015, Nature, 521, 495
- Mignard, F. & Klioner, S. 2012, A&A, 547, A59
- Mignard, F., Klioner, S., Lindegren, L., Bastian, U., Bombrun, A., Hernndez, J., Hobbs, D., Lammers, U., Michalik, D., Ramos-Lerate, M., Biermann, M., Butkevich, A., Comoretto, G., Joliet, E., Holl, B., Hutton, A., Parsons, P., Steidelmler, H., Andrei, A., Bourda, G., & Charlot, P. 2016, A&A, 595, A5
- Newville, M., Stensitzki, T., Allen, D. B., & Ingargiola, A. 2014, Zenodo, <http://doi.org/10.5281/zenodo.11813>
- Paine, J., Darling, J., & Truebenbach, A. E. 2018, ApJ, in press (arXiv:1804.02064)
- Petrov, L. & Kovalev, Y. Y. 2017, MNRAS, 467, L71
- Pyne, T., Gwinn, C. R., Birkinshaw, M., Eubanks, T. M., & Matsakis, D. N. 1996, ApJ, 465, 566

- Reid, M. J., Menten, K. M., Brunthaler, A., Zheng, X. W., Dame, T. M., Xu, Y., Wu, Y., Zhang, B., Sanna, A., Sato, M., Hachisuka, K., Choi, Y. K., Immer, K., Moscadelli, L., Rygl, K. L. J., & Bartkiewicz, A. 2014, *ApJ*, 783, 130
- Robin, A. C., Luri, X., Reylé, C., Isasi, Y., Grux, E., Blanco-Cuaresma, S., Arenou, F., Babusiaux, C., Belcheva, M., Drimmel, R., Jordi, C., Krone-Martins, A., Masana, E., Mauduit, J. C., Mignard, F., Mowlavi, N., Rocca-Volmerange, B., Sartoretti, P., Slezak, E., & Sozzetti, A. 2012, *A&A*, 543, A100
- Seljak, U. & Zaldarriaga, M. 1997, *PhRvL*, 78, 2054
- Sivia, D. S. & Skilling, J. 2006, Oxford University Press, 2nd edition
- Smith, T. L., Pierpaoli, E., & Kamionkowski, M. 2006, *PhRvL*, 97, 021301
- Souchay, J., Andrei, A. H., Barache, C., Kalewicz, T., Gattano, C., Coelho, B., Taris, F., Bouquillon, S., & Becker, O. 2015, *A&A*, 583, A75
- Thorne, K. S. 1980, *Reviews of Modern Physics*, 52, 299
- Titov, O., Lambert, S. B., & Gontier, A.-M. 2011, *A&A*, 529, A91
- Titov, O. & Lambert, S. 2013, *A&A*, 559, A95
- Titov, O. & Lambert, S. 2016, arxiv, 1603.09416
- Truebenbach, A. E. & Darling, J. 2017, *ApJS*, 233, 3
- Wills, D. & Wills, B. J. 1976, *ApJS*, 31, 143
- Xu, M. H., Wang, G. L., & Zhao, M. 2013, *MNRAS*, 430, 2633

APPENDIX

A. VECTOR SPHERICAL HARMONICS

Here we present explicit formulae for the $\ell \leq 3$ vector spherical harmonics that are based on those described in Mignard & Klioner (2012) but which have strictly real coefficients (and therefore have sign differences) and explicitly include factors of 2 that are needed for correct power calculations.

The vector spherical harmonics for the electric and magnetic dipoles described by Mignard & Klioner (2012) and listed in Tables 4 and 5 are

$$\begin{aligned}\vec{\mathbf{V}}_{E1}(\alpha, \delta) = & \left(s_{11}^{Re} \frac{1}{2} \sqrt{\frac{3}{\pi}} \sin \alpha + s_{11}^{Im} \frac{1}{2} \sqrt{\frac{3}{\pi}} \cos \alpha \right) \hat{\mathbf{e}}_\alpha \\ & + \left(s_{10} \frac{1}{2} \sqrt{\frac{3}{2\pi}} \cos \delta + s_{11}^{Re} \frac{1}{2} \sqrt{\frac{3}{\pi}} \cos \alpha \sin \delta - s_{11}^{Im} \frac{1}{2} \sqrt{\frac{3}{\pi}} \sin \alpha \sin \delta \right) \hat{\mathbf{e}}_\delta\end{aligned}\quad (\text{A1})$$

and

$$\begin{aligned}\vec{\mathbf{V}}_{M1}(\alpha, \delta) = & \left(t_{10} \frac{1}{2} \sqrt{\frac{3}{2\pi}} \cos \delta + t_{11}^{Re} \frac{1}{2} \sqrt{\frac{3}{\pi}} \cos \alpha \sin \delta - t_{11}^{Im} \frac{1}{2} \sqrt{\frac{3}{\pi}} \sin \alpha \sin \delta \right) \hat{\mathbf{e}}_\alpha \\ & + \left(-t_{11}^{Re} \frac{1}{2} \sqrt{\frac{3}{\pi}} \sin \alpha - t_{11}^{Im} \frac{1}{2} \sqrt{\frac{3}{\pi}} \cos \alpha \right) \hat{\mathbf{e}}_\delta,\end{aligned}\quad (\text{A2})$$

where the $s_{\ell m}$ are the amplitudes of the spheroidal (curl-free or E-mode) orders, the $t_{\ell m}$ are the amplitudes of the toroidal (divergence-less or B-mode) orders, and $\hat{\mathbf{e}}_\alpha$ and $\hat{\mathbf{e}}_\delta$ are the unit vectors in the right ascension and declination directions, respectively.

The quadrupole vector spherical harmonics are

$$\begin{aligned}\vec{\mathbf{V}}_{E2}(\alpha, \delta) = & \left(s_{21}^{Re} \frac{1}{2} \sqrt{\frac{5}{\pi}} \sin \alpha \sin \delta + s_{21}^{Im} \frac{1}{2} \sqrt{\frac{5}{\pi}} \cos \alpha \sin \delta - s_{22}^{Re} \frac{1}{2} \sqrt{\frac{5}{\pi}} \sin 2\alpha \cos \delta \right. \\ & \left. - s_{22}^{Im} \frac{1}{2} \sqrt{\frac{5}{\pi}} \cos 2\alpha \cos \delta \right) \hat{\mathbf{e}}_\alpha \\ & + \left(s_{20} \frac{1}{4} \sqrt{\frac{15}{2\pi}} \sin 2\delta - s_{21}^{Re} \frac{1}{2} \sqrt{\frac{5}{\pi}} \cos \alpha \cos 2\delta + s_{21}^{Im} \frac{1}{2} \sqrt{\frac{5}{\pi}} \sin \alpha \cos 2\delta \right. \\ & \left. - s_{22}^{Re} \frac{1}{4} \sqrt{\frac{5}{\pi}} \cos 2\alpha \sin 2\delta + s_{22}^{Im} \frac{1}{4} \sqrt{\frac{5}{\pi}} \sin 2\alpha \sin 2\delta \right) \hat{\mathbf{e}}_\delta\end{aligned}\quad (\text{A3})$$

and

$$\begin{aligned}\vec{\mathbf{V}}_{M2}(\alpha, \delta) = & \left(t_{20} \frac{1}{4} \sqrt{\frac{15}{2\pi}} \sin 2\delta - t_{21}^{Re} \frac{1}{2} \sqrt{\frac{5}{\pi}} \cos \alpha \cos 2\delta + t_{21}^{Im} \frac{1}{2} \sqrt{\frac{5}{\pi}} \sin \alpha \cos 2\delta \right. \\ & \left. - t_{22}^{Re} \frac{1}{4} \sqrt{\frac{5}{\pi}} \cos 2\alpha \sin 2\delta + t_{22}^{Im} \frac{1}{4} \sqrt{\frac{5}{\pi}} \sin 2\alpha \sin 2\delta \right) \hat{\mathbf{e}}_\alpha \\ & + \left(-t_{21}^{Re} \frac{1}{2} \sqrt{\frac{5}{\pi}} \sin \alpha \sin \delta - t_{21}^{Im} \frac{1}{2} \sqrt{\frac{5}{\pi}} \cos \alpha \sin \delta + t_{22}^{Re} \frac{1}{2} \sqrt{\frac{5}{\pi}} \sin 2\alpha \cos \delta \right. \\ & \left. + t_{22}^{Im} \frac{1}{2} \sqrt{\frac{5}{\pi}} \cos 2\alpha \cos \delta \right) \hat{\mathbf{e}}_\delta.\end{aligned}\quad (\text{A4})$$

The octopole ($\ell = 3$) vector spherical harmonics are

$$\vec{\mathbf{V}}_{E3}(\alpha, \delta) = \left(s_{31}^{Re} \frac{1}{8} \sqrt{\frac{7}{\pi}} \sin \alpha (5 \sin^2 \delta - 1) + s_{31}^{Im} \frac{1}{8} \sqrt{\frac{7}{\pi}} \cos \alpha (5 \sin^2 \delta - 1) \right)$$

$$\begin{aligned}
& - s_{32}^{Re} \frac{1}{4} \sqrt{\frac{35}{2\pi}} \sin 2\alpha \sin 2\delta - s_{32}^{Im} \frac{1}{4} \sqrt{\frac{35}{2\pi}} \cos 2\alpha \sin 2\delta + s_{33}^{Re} \frac{1}{8} \sqrt{\frac{105}{\pi}} \sin 3\alpha \cos^2 \delta \\
& \quad + s_{33}^{Im} \frac{1}{8} \sqrt{\frac{105}{\pi}} \cos 3\alpha \cos^2 \delta \Big) \hat{\mathbf{e}}_\alpha \\
& + \left(s_{30} \frac{1}{8} \sqrt{\frac{21}{\pi}} (5 \sin^2 \delta - 1) \cos \delta + s_{31}^{Re} \frac{1}{8} \sqrt{\frac{7}{\pi}} \cos \alpha \sin \delta (15 \sin^2 \delta - 11) \right. \\
& - s_{31}^{Im} \frac{1}{8} \sqrt{\frac{7}{\pi}} \sin \alpha \sin \delta (15 \sin^2 \delta - 11) - s_{32}^{Re} \frac{1}{4} \sqrt{\frac{35}{2\pi}} \cos 2\alpha \cos \delta (3 \sin^2 \delta - 1) \\
& \quad + s_{32}^{Im} \frac{1}{4} \sqrt{\frac{35}{2\pi}} \sin 2\alpha \cos \delta (3 \sin^2 \delta - 1) + s_{33}^{Re} \frac{1}{8} \sqrt{\frac{105}{\pi}} \cos 3\alpha \cos^2 \delta \sin \delta \\
& \quad \left. - s_{33}^{Im} \frac{1}{8} \sqrt{\frac{105}{\pi}} \sin 3\alpha \cos^2 \delta \sin \delta \right) \hat{\mathbf{e}}_\delta \tag{A5}
\end{aligned}$$

and

$$\begin{aligned}
\vec{\mathbf{V}}_{M3}(\alpha, \delta) = & \left(t_{30} \frac{1}{8} \sqrt{\frac{21}{\pi}} (5 \sin^2 \delta - 1) \cos \delta + t_{31}^{Re} \frac{1}{8} \sqrt{\frac{7}{\pi}} \cos \alpha \sin \delta (15 \sin^2 \delta - 11) \right. \\
& - t_{31}^{Im} \frac{1}{8} \sqrt{\frac{7}{\pi}} \sin \alpha \sin \delta (15 \sin^2 \delta - 11) - t_{32}^{Re} \frac{1}{4} \sqrt{\frac{35}{2\pi}} \cos 2\alpha \cos \delta (3 \sin^2 \delta - 1) \\
& + t_{32}^{Im} \frac{1}{4} \sqrt{\frac{35}{2\pi}} \sin 2\alpha \cos \delta (3 \sin^2 \delta - 1) + t_{33}^{Re} \frac{1}{8} \sqrt{\frac{105}{\pi}} \cos 3\alpha \cos^2 \delta \sin \delta \\
& \quad \left. - t_{33}^{Im} \frac{1}{8} \sqrt{\frac{105}{\pi}} \sin 3\alpha \cos^2 \delta \sin \delta \right) \hat{\mathbf{e}}_\alpha \\
& + \left(- t_{31}^{Re} \frac{1}{8} \sqrt{\frac{7}{\pi}} \sin \alpha (5 \sin^2 \delta - 1) - t_{31}^{Im} \frac{1}{8} \sqrt{\frac{7}{\pi}} \cos \alpha (5 \sin^2 \delta - 1) \right. \\
& + t_{32}^{Re} \frac{1}{4} \sqrt{\frac{35}{2\pi}} \sin 2\alpha \sin 2\delta + t_{32}^{Im} \frac{1}{4} \sqrt{\frac{35}{2\pi}} \cos 2\alpha \sin 2\delta \\
& \quad \left. - t_{33}^{Re} \frac{1}{8} \sqrt{\frac{105}{\pi}} \sin 3\alpha \cos^2 \delta - t_{33}^{Im} \frac{1}{8} \sqrt{\frac{105}{\pi}} \cos 3\alpha \cos^2 \delta \right) \hat{\mathbf{e}}_\delta. \tag{A6}
\end{aligned}$$

Table 4. Spheroidal (E-mode) Vector Spherical Harmonics ($\ell \leq 3$)

ℓ, m	Amplitude	$\hat{\mathbf{e}}_\alpha$	$\hat{\mathbf{e}}_\delta$
1,0	$\frac{1}{2} \sqrt{\frac{3}{2\pi}}$	0	$\cos \delta$
1,1 (Re)	$\frac{1}{2} \sqrt{\frac{3}{\pi}}$	$\sin \alpha$	$\cos \alpha \sin \delta$
1,1 (Im)	$\frac{1}{2} \sqrt{\frac{3}{\pi}}$	$\cos \alpha$	$-\sin \alpha \sin \delta$
2,0	$\frac{1}{4} \sqrt{\frac{15}{2\pi}}$	0	$\sin 2\delta$
2,1 (Re)	$\frac{1}{2} \sqrt{\frac{5}{\pi}}$	$\sin \alpha \sin \delta$	$-\cos \alpha \cos 2\delta$
2,1 (Im)	$\frac{1}{2} \sqrt{\frac{5}{\pi}}$	$\cos \alpha \sin \delta$	$\sin \alpha \cos 2\delta$
2,2 (Re)	$\frac{1}{4} \sqrt{\frac{5}{\pi}}$	$-2 \sin 2\alpha \cos \delta$	$-\cos 2\alpha \sin 2\delta$
2,2 (Im)	$\frac{1}{4} \sqrt{\frac{5}{\pi}}$	$-2 \cos 2\alpha \cos \delta$	$\sin 2\alpha \sin 2\delta$
3,0	$\frac{1}{8} \sqrt{\frac{21}{\pi}}$	0	$(5 \sin^2 \delta - 1) \cos \delta$
3,1 (Re)	$\frac{1}{8} \sqrt{\frac{7}{\pi}}$	$\sin \alpha (5 \sin^2 \delta - 1)$	$\cos \alpha \sin \delta (15 \sin^2 \delta - 11)$
3,1 (Im)	$\frac{1}{8} \sqrt{\frac{7}{\pi}}$	$\cos \alpha (5 \sin^2 \delta - 1)$	$-\sin \alpha \sin \delta (15 \sin^2 \delta - 11)$
3,2 (Re)	$\frac{1}{4} \sqrt{\frac{35}{2\pi}}$	$-\sin 2\alpha \sin 2\delta$	$-\cos 2\alpha \cos \delta (3 \sin^2 \delta - 1)$
3,2 (Im)	$\frac{1}{4} \sqrt{\frac{35}{2\pi}}$	$-\cos 2\alpha \sin 2\delta$	$\sin 2\alpha \cos \delta (3 \sin^2 \delta - 1)$
3,3 (Re)	$\frac{1}{8} \sqrt{\frac{105}{\pi}}$	$\sin 3\alpha \cos^2 \delta$	$\cos 3\alpha \cos^2 \delta \sin \delta$
3,3 (Im)	$\frac{1}{8} \sqrt{\frac{105}{\pi}}$	$\cos 3\alpha \cos^2 \delta$	$-\sin 3\alpha \cos^2 \delta \sin \delta$

Table 5. Toroidal (B-mode) Vector Spherical Harmonics ($\ell \leq 3$)

ℓ, m	Amplitude	$\hat{\mathbf{e}}_\alpha$	$\hat{\mathbf{e}}_\delta$
1,0	$\frac{1}{2} \sqrt{\frac{3}{2\pi}}$	$\cos \delta$	0
1,1 (Re)	$\frac{1}{2} \sqrt{\frac{3}{\pi}}$	$\cos \alpha \sin \delta$	$-\sin \alpha$
1,1 (Im)	$\frac{1}{2} \sqrt{\frac{3}{\pi}}$	$-\sin \alpha \sin \delta$	$-\cos \alpha$
2,0	$\frac{1}{4} \sqrt{\frac{15}{2\pi}}$	$\sin 2\delta$	0
2,1 (Re)	$\frac{1}{2} \sqrt{\frac{5}{\pi}}$	$-\cos \alpha \cos 2\delta$	$-\sin \alpha \sin \delta$
2,1 (Im)	$\frac{1}{2} \sqrt{\frac{5}{\pi}}$	$\sin \alpha \cos 2\delta$	$-\cos \alpha \sin \delta$
2,2 (Re)	$\frac{1}{4} \sqrt{\frac{5}{\pi}}$	$-\cos 2\alpha \sin 2\delta$	$2 \sin 2\alpha \cos \delta$
2,2 (Im)	$\frac{1}{4} \sqrt{\frac{5}{\pi}}$	$\sin 2\alpha \sin 2\delta$	$2 \cos 2\alpha \cos \delta$
3,0	$\frac{1}{8} \sqrt{\frac{21}{\pi}}$	$(5 \sin^2 \delta - 1) \cos \delta$	0
3,1 (Re)	$\frac{1}{8} \sqrt{\frac{7}{\pi}}$	$\cos \alpha \sin \delta (15 \sin^2 \delta - 11)$	$-\sin \alpha (5 \sin^2 \delta - 1)$
3,1 (Im)	$\frac{1}{8} \sqrt{\frac{7}{\pi}}$	$-\sin \alpha \sin \delta (15 \sin^2 \delta - 11)$	$-\cos \alpha (5 \sin^2 \delta - 1)$
3,2 (Re)	$\frac{1}{4} \sqrt{\frac{35}{2\pi}}$	$-\cos 2\alpha \cos \delta (3 \sin^2 \delta - 1)$	$\sin 2\alpha \sin 2\delta$
3,2 (Im)	$\frac{1}{4} \sqrt{\frac{35}{2\pi}}$	$\sin 2\alpha \cos \delta (3 \sin^2 \delta - 1)$	$\cos 2\alpha \sin 2\delta$
3,3 (Re)	$\frac{1}{8} \sqrt{\frac{105}{\pi}}$	$\cos 3\alpha \cos^2 \delta \sin \delta$	$-\sin 3\alpha \cos^2 \delta$
3,3 (Im)	$\frac{1}{8} \sqrt{\frac{105}{\pi}}$	$-\sin 3\alpha \cos^2 \delta \sin \delta$	$-\cos 3\alpha \cos^2 \delta$

B. VLBA+GAIA ASTROMETRY AND PROPER MOTIONS

Table 6 lists the objects that show significant and consistent radio and optical proper motion. Based on the amplitudes of the proper motions, these are most likely intrinsic and associated with jets. Objects showing apparent superluminal motions are indicated in bold, as are the superluminal velocity components and amplitudes.

Table 7 lists the *Gaia* 2015.0 epoch J2000 coordinates, the VLBA-only and VLBA+*Gaia* proper motions obtained from the time series fits described in Section 3.2, and the *Gaia*-VLBA coordinate offset in *Gaia* standard deviations. The VLBA proper motions were obtained from bootstrap-resampled time series and may differ slightly from — but are statistically consistent with — the [Truebenbach & Darling \(2017\)](#) proper motion catalog. The VLBA+*Gaia* proper motion catalog in Table 7 forms a subset of the VLBA-only [Truebenbach & Darling \(2017\)](#) catalog because not all radio sources have *Gaia* counterparts.

Table 6. Objects Showing Significant Consistent Radio and Optical Proper Motion

Name	VLBA+Gaia PM		Redshift ^a (Mpc)	D_M (Mpc)	Apparent Velocity		
	μ_α (mas yr ⁻¹)	μ_δ (mas yr ⁻¹)			v_α (c)	v_δ (c)	v_{Total} (c)
0007+171	136.6(25.4)	-0.3(12.4)	1.60	4654	10.1(1.9)	-0.02(0.91)	10.1(1.9)
0016+731	5.5(1.1)	5.1(0.7)	1.78	4969	-0.43(0.09)	0.40(0.06)	0.59(0.07)
0059+581	7.5(0.4)	2.8(0.5)	0.64	2359	-0.28(0.01)	-0.10(0.02)	0.30(0.02)
0119+041	9.2(1.8)	6.0(1.9)	0.64	2359	-0.34(0.07)	0.22(0.07)	0.41(0.07)
0229+131	10.7(0.7)	7.0(0.7)	2.06	5409	0.92(0.06)	0.60(0.06)	1.09(0.06)
NRAO150	6.0(1.9)	16.6(2.3)	1.52	4505	0.43(0.14)	1.18(0.16)	1.26(0.16)
0420-014	-5.5(0.7)	-8.5(0.9)	0.92	3158	-0.27(0.03)	-0.42(0.04)	0.51(0.04)
NRAO190	-20.6(9.9)	-28.6(3.3)	0.84	2943	-0.96(0.46)	-1.33(0.15)	1.64(0.30)
0454-234	-3.8(0.7)	-7.1(0.8)	1.00	3365	-0.20(0.04)	-0.38(0.04)	0.43(0.04)
0458-020	-2.5(0.9)	-10.4(0.8)	2.29	5731	-0.23(0.08)	-0.94(0.07)	0.97(0.07)
0454+844	6.9(4.7)	19.7(3.0)	1.34	4145	0.45(0.31)	1.29(0.20)	1.37(0.21)
0552+398	0.2(0.4)	-3.5(0.4)	2.37	5835	0.02(0.04)	-0.32(0.04)	0.32(0.04)
0602+673	0.5(0.8)	20.4(1.2)	1.97	5274	0.04(0.07)	1.70(0.10)	1.70(0.10)
0657+172	7.2(1.4)	-5.4(1.9)	1.08	3562	0.41(0.08)	-0.30(0.11)	0.51(0.09)
0723-008	-50.0(6.5)	107.5(13.1)	0.13	542	-0.43(0.06)	0.92(0.11)	1.02(0.10)
0743+259	-3.5(2.8)	-33.4(3.6)	2.99	6543	-0.36(0.29)	-3.46(0.37)	3.47(0.37)
0805+410	5.4(1.1)	9.4(1.3)	1.42	4309	0.37(0.07)	0.64(0.09)	0.74(0.09)
1038+064	-15.1(3.5)	61.6(8.4)	1.27	3996	-0.95(0.22)	3.89(0.53)	4.01(0.52)
1045-188	22.3(4.3)	-73.5(10.4)	0.59	2202	0.78(0.15)	-2.56(0.36)	2.67(0.35)
1053+815	-7.1(1.4)	1.8(1.5)	0.71	2571	-0.29(0.06)	0.07(0.06)	0.30(0.06)
1057-797	0.5(1.3)	-7.5(1.2)	0.58	2170	0.02(0.04)	-0.26(0.04)	0.26(0.04)
1104-445	-20.1(3.0)	12.4(3.2)	1.60	4654	-1.48(0.22)	0.91(0.24)	1.74(0.22)
1124-186	1.7(1.1)	-6.8(1.2)	1.05	3489	0.09(0.06)	-0.38(0.07)	0.39(0.07)
1219+044	6.3(1.1)	-3.6(2.0)	0.97	3288	0.33(0.06)	-0.19(0.10)	0.38(0.07)
1300+580	5.2(0.7)	11.4(0.8)	1.09	3586	0.29(0.04)	0.65(0.05)	0.71(0.04)
1342+663	-40.9(7.3)	-9.8(2.8)	1.35	4166	-2.69(0.48)	-0.65(0.18)	2.77(0.47)
1424-418	-9.8(1.6)	2.0(1.8)	1.52	4505	-0.70(0.11)	0.14(0.13)	0.71(0.11)
1606+106	5.4(1.0)	0.1(0.9)	1.23	3908	0.32(0.06)	0.01(0.06)	0.32(0.06)
1622-253	-0.2(1.1)	8.0(1.4)	0.79	2803	-0.01(0.05)	0.35(0.06)	0.35(0.06)
1642+690	6.3(1.6)	-19.3(3.0)	0.75	2688	0.27(0.07)	-0.82(0.13)	0.86(0.12)
1657-562 ^b	33.7(10.1)	-110.7(17.0)
NRAO530	7.4(1.3)	7.2(2.3)	0.90	3105	0.36(0.06)	0.35(0.11)	0.51(0.09)
1745+624	10.7(1.5)	10.4(2.2)	3.89	7328	1.24(0.17)	1.21(0.25)	1.73(0.22)
1846+322	-29.5(4.7)	7.2(5.9)	0.80	2831	-1.32(0.21)	0.32(0.26)	1.36(0.21)
3C395	66.2(9.9)	-32.1(6.9)	0.64	2359	2.47(0.37)	-1.20(0.26)	2.74(0.35)
1923+210 ^b	10.0(2.4)	17.9(1.4)
1958-179	-7.7(1.0)	-4.0(1.4)	0.65	2390	-0.29(0.04)	-0.15(0.05)	0.33(0.04)
2007+777	22.8(3.0)	-0.0(1.5)	0.34	1350	0.49(0.06)	-0.00(0.03)	0.49(0.06)
3C418	-15.3(1.2)	-7.7(1.6)	1.69	4815	-1.16(0.09)	-0.59(0.12)	1.30(0.10)
2059+034	-5.3(3.5)	-25.0(3.8)	1.01	3390	-0.28(0.19)	-1.34(0.20)	1.37(0.20)
2126-158	-10.6(2.5)	-66.5(5.2)	3.27	6812	-1.14(0.27)	-7.16(0.56)	7.25(0.55)
2155-152	-30.4(6.3)	-40.1(7.3)	0.67	2451	-1.18(0.24)	-1.55(0.28)	1.95(0.27)
2209+236	21.7(2.0)	2.6(2.0)	1.13	3680	1.26(0.12)	0.15(0.12)	1.27(0.12)
2214+350	5.6(3.1)	-69.5(5.0)	0.51	1942	0.17(0.10)	-2.13(0.15)	2.14(0.15)
2229+695	39.3(3.3)	4.8(1.6)	1.41	4289	2.67(0.22)	0.33(0.11)	2.69(0.22)

NOTE—Parenthetical values are 1σ uncertainties. Apparent velocities are in the rest frame of each object, in units of the speed of light, c (see Section 3.2). Bold type indicates the names and velocities of objects showing superluminal motion.

^a Redshifts were obtained from the Optical Characteristic of Astrometric Radio Sources Catalog (OCARS; [Malkin 2016](#)), except for 0723-008, which was obtained from the NASA/IPAC Extragalactic Database (NED).

^b 1657-562 and 1923+210 show VLBA+*Gaia* astrometric correspondence and significant proper motion, but the redshifts for these objects are unknown. If they have redshifts greater than 0.13 and 0.90, respectively, then their observed proper motions would be superluminal.

Table 7. VLBA+*Gaia* Astrometry and Proper Motions

Name	Gaia 2015.0 Coordinates		VLBA PM		VLBA+Gaia PM		Gaia-VLBA Offset	
	RA (J2000)	Dec (J2000)	μ_α	μ_δ	μ_α	μ_δ	$\Delta\alpha$	$\Delta\delta$
	(h:m:s)	(d:m:s)	(mas yr $^{-1}$)	(σ)	(σ)			
0002–478	00:04:35.65554(6)	−47:36:19.6040(8)	−23.1(13.2)	−46.5(20.0)	−22.9(13.2)	−47.4(19.8)	1.1	0.2
0003+380	00:05:57.17593(8)	+38:20:15.1435(4)	−15.4(9.9)	−1.5(11.3)	−12.6(9.2)	−18.9(13.6)	6.7	14.2
0003–066	00:06:13.89290(2)	−06:23:35.3351(1)	0.3(1.3)	3.7(1.8)	0.4(1.3)	3.5(1.8)	0.4	1.4
IIIZW2	00:10:31.00592(2)	+10:58:29.5038(2)	2.3(12.3)	−9.7(11.8)	3.3(11.5)	−13.1(12.0)	0.9	2.2
0007+171	00:10:33.99072(4)	+17:24:18.7609(3)	136.2(27.2)	9.8(14.7)	136.6(25.4)	−0.3(12.4)	0.6	2.0
0008–264	00:11:01.24678(3)	−26:12:33.3768(3)	1.1(6.8)	−0.4(8.2)	1.2(6.9)	−1.5(8.3)	1.3	0.8
0010+405	00:13:31.13019(11)	+40:51:37.1457(6)	−3.9(3.1)	7.2(4.6)	−3.6(3.0)	7.7(4.7)	0.1	2.6
0013–005	00:16:11.08856(9)	−00:15:12.4450(7)	1.8(5.3)	3.6(7.3)	1.6(4.8)	3.3(7.8)	0.0	0.5
0017+200	00:19:37.85451(8)	+20:21:45.6452(12)	−19.2(9.0)	−0.9(4.7)	−18.4(9.4)	−0.5(4.3)	0.2	0.5
0016+731	00:19:45.78609(19)	+73:27:30.0178(4)	−5.4(1.0)	5.0(0.7)	−5.5(1.1)	5.1(0.7)	1.5	0.3
0019+058	00:22:32.44119(4)	+06:08:04.2688(3)	−3.9(4.8)	−1.3(7.3)	−3.9(4.6)	−1.8(7.3)	0.6	0.5
0025+197	00:28:29.81863(29)	+20:00:26.7435(18)	10.6(6.3)	−0.8(10.4)	10.8(5.8)	−0.0(10.4)	0.5	0.3
0035–252	00:38:14.73547(4)	−24:59:02.2350(3)	−8.6(10.4)	−2.2(18.5)	−9.9(10.2)	−2.1(18.1)	0.7	0.8
0035+413	00:38:24.84381(30)	+41:37:05.9997(49)	−6.3(5.3)	−2.4(11.4)	−6.3(5.0)	−2.8(10.8)	0.8	0.1
NGC0262	00:48:47.14200(26)	+31:57:25.0441(33)	8.9(10.5)	−92.6(45.9)	8.7(10.2)	−92.2(43.5)	2.0	12.1
0047+023	00:49:43.23593(4)	+02:37:03.7786(4)	0.3(9.8)	29.6(18.7)	0.2(11.1)	29.2(21.2)	0.2	0.0
0047–579	00:49:59.47304(3)	−57:38:27.3398(3)	−33.8(16.3)	−29.4(25.4)	−28.2(10.3)	−10.2(18.8)	1.2	2.1
0048–097	00:50:41.31733(4)	−09:29:05.2107(5)	−3.6(1.2)	−5.2(1.2)	−3.7(1.2)	−5.2(1.2)	1.5	0.7
0048–427	00:51:09.50186(3)	−42:26:33.2935(2)	4.3(11.6)	47.0(17.8)	5.0(11.9)	45.2(16.7)	1.5	1.7
0054+161	00:56:55.29431(10)	+16:25:13.3418(10)	4.1(7.2)	1.1(10.8)	4.4(7.2)	1.1(10.5)	0.3	0.9
0055–059	00:58:05.06630(2)	−05:39:52.2782(3)	0.9(8.7)	8.2(24.1)	1.2(7.6)	8.1(23.4)	0.3	0.6
0056–572	00:58:46.58119(3)	−56:59:11.4705(2)	11.8(19.5)	24.2(43.6)	17.1(51.9)	21.0(42.8)	1.2	1.4
0056–001	00:59:05.51495(3)	+00:06:51.6214(2)	30.5(50.2)	−57.1(59.5)	27.9(27.2)	−14.7(20.5)	0.5	5.0
0059+581	01:02:45.76238(3)	+58:24:11.1368(3)	−7.5(0.5)	−2.8(0.5)	−7.5(0.4)	−2.8(0.5)	0.4	0.7
0104–408	01:06:45.10791(11)	−40:34:19.9605(7)	−0.1(1.7)	−2.0(2.2)	−0.0(1.9)	−2.0(2.2)	0.5	0.3
0109+224	01:12:05.82471(2)	+22:44:38.7862(2)	−2.8(4.1)	−7.9(5.5)	−2.7(4.0)	−8.5(5.3)	0.2	0.8
0110+495	01:13:27.00688(17)	+49:48:24.0435(9)	−8.8(5.5)	16.7(6.4)	−9.0(5.7)	16.2(6.4)	0.4	0.2
0111+021	01:13:43.14516(10)	+02:22:17.3128(7)	3.4(3.2)	−3.7(3.8)	3.4(3.3)	−4.4(3.9)	2.1	4.7
0112–017	01:15:17.09994(3)	−01:27:04.5774(3)	−42.1(33.7)	5.3(15.1)	−43.7(30.8)	5.2(13.5)	1.3	0.6
0113–118	01:16:12.52200(3)	−11:36:15.4344(3)	−13.0(7.5)	−14.4(17.9)	−13.9(7.8)	−11.0(15.1)	0.6	1.2
0115–214	01:17:48.78013(4)	−21:11:06.6324(4)	7.1(4.4)	−4.2(7.6)	6.7(4.6)	−4.0(7.7)	0.1	2.0
0116–219	01:18:57.26217(2)	−21:41:30.1404(2)	19.3(8.7)	−31.9(13.3)	19.2(8.7)	−31.7(13.4)	0.7	0.5
0118–272	01:20:31.66311(2)	−27:01:24.6459(2)	15.2(60.4)	37.3(70.1)	−192.5(31.1)	485.6(45.6)	17.9	32.5
0119+115	01:21:41.59517(9)	+11:49:50.4204(7)	6.2(1.1)	50.8(2.6)	6.2(1.0)	51.2(2.3)	1.3	9.7
0119+041	01:21:56.86171(9)	+04:22:24.7346(6)	−9.1(1.8)	5.9(2.0)	−9.2(1.8)	6.0(1.9)	0.2	0.3
0122–003	01:25:28.84387(2)	−00:05:55.9316(2)	34.8(381.9)	29.3(395.2)	35.2(128.0)	42.6(171.5)	0.1	1.8
0123+257	01:26:42.79264(5)	+25:59:01.3001(4)	−8.1(5.4)	−11.2(16.3)	−8.0(4.8)	−11.4(13.5)	0.1	0.0
0130–171	01:32:43.48741(2)	−16:54:48.5224(2)	−13.0(10.8)	21.4(14.4)	−21.9(10.0)	−4.4(8.6)	1.8	3.5
0131–522	01:33:05.76257(2)	−52:00:03.9460(2)	−20.9(9.0)	51.8(12.6)	−21.8(8.8)	52.2(13.1)	2.7	2.5
0133+476	01:36:58.59481(5)	+47:51:29.0998(5)	−1.6(0.7)	1.8(0.7)	−1.5(0.7)	1.9(0.7)	0.0	0.6
0135–247	01:37:38.34641(2)	−24:30:53.8857(1)	−10.7(21.0)	10.6(13.4)	−15.3(17.1)	−3.7(6.8)	1.5	2.7
3C48	01:37:41.29963(2)	+33:09:35.0800(2)	99.8(388.9)	−680.5(857.8)	75.9(32.4)	−2284.5(46.0)	2.3	159.4
0138–097	01:41:25.83216(3)	−09:28:43.6750(3)	−5.0(10.1)	6.1(10.3)	−6.0(9.7)	5.6(9.7)	0.1	2.4
0149+218	01:52:18.05905(7)	+22:07:07.7007(5)	0.2(3.1)	3.2(4.2)	0.1(2.8)	3.5(4.5)	0.1	1.6
0150–334	01:53:10.12171(1)	−33:10:25.8619(2)	39.4(46.5)	4.8(35.1)	−22.0(33.5)	5.3(12.7)	6.6	0.2

Table 7 continued

Table 7 (*continued*)

Name	Gaia 2015.0 Coordinates		VLBA PM		VLBA+Gaia PM		Gaia-VLBA Offset	
	RA (J2000)	Dec (J2000)	μ_α	μ_δ	μ_α	μ_δ	$\Delta\alpha$	$\Delta\delta$
			(h:m:s)	(d:m:s)	(mas yr $^{-1}$)	(mas yr $^{-1}$)	(σ)	(σ)
0153+744	01:57:34.96488(9)	+74:42:43.2285(3)	-10.5(10.7)	-25.6(19.9)	-10.7(8.6)	-35.5(19.3)	0.1	3.1
0159+723	02:03:33.38509(13)	+72:32:53.6677(6)	-10.6(4.8)	1.6(4.4)	-10.9(5.3)	1.2(4.6)	1.1	0.6
0201+113	02:03:46.65695(63)	+11:34:45.4099(34)	0.5(1.7)	-10.8(3.0)	0.7(1.8)	-10.6(3.0)	0.2	0.2
0202-172	02:04:57.67433(2)	-17:01:19.8409(3)	-12.3(4.1)	-14.7(10.5)	-12.4(4.2)	-15.1(10.5)	0.2	0.6
0202+319	02:05:04.92541(5)	+32:12:30.0949(3)	4.5(2.0)	1.7(3.2)	4.2(2.0)	1.6(3.4)	0.8	1.5
0215+015	02:17:48.95475(8)	+01:44:49.6986(7)	1.5(3.3)	-10.0(4.7)	1.8(3.4)	-9.8(4.7)	0.0	0.6
0219+428	02:22:39.61146(2)	+43:02:07.7985(2)	-6.9(11.1)	17.6(12.8)	-10.2(8.2)	7.0(10.8)	1.7	3.2
0220-349	02:22:56.40162(24)	-34:41:28.7299(29)	-1.5(9.0)	2.8(8.2)	-1.5(8.5)	2.1(7.6)	0.1	0.1
0221+067	02:24:28.42817(5)	+06:59:23.3421(6)	-8.6(4.0)	-5.9(6.1)	-8.4(4.3)	-6.2(6.3)	0.3	1.0
4C67.05	02:28:50.05149(9)	+67:21:03.0297(4)	-5.1(2.3)	-8.3(5.0)	-4.9(2.3)	-8.0(4.7)	0.1	1.0
0227-369	02:29:28.44913(6)	-36:43:56.8233(9)	7.0(12.6)	-17.6(12.9)	7.6(13.1)	-20.5(13.0)	1.1	1.1
0230-790	02:29:34.94712(30)	-78:47:45.6017(6)	2.4(5.8)	22.8(9.3)	2.2(6.2)	23.9(9.4)	1.7	0.1
0229+131	02:31:45.89404(7)	+13:22:54.7158(7)	10.7(0.7)	7.0(0.7)	10.7(0.7)	7.0(0.7)	0.4	0.9
0234-301	02:36:31.16944(2)	-29:53:55.5401(3)	-33.6(14.4)	-7.0(18.6)	-32.0(15.3)	-5.2(19.1)	1.1	2.0
0235-618	02:36:53.24547(10)	-61:36:15.1844(9)	-0.3(16.3)	22.6(20.1)	-6.0(17.1)	18.9(20.5)	2.7	0.9
0234+285	02:37:52.40567(3)	+28:48:08.9903(3)	4.0(0.9)	-0.7(1.3)	3.9(1.0)	-0.8(1.3)	0.5	0.9
0237-027	02:39:45.47289(52)	-02:34:40.9184(32)	8.7(3.7)	-11.1(7.3)	9.1(3.6)	-11.1(7.0)	1.2	1.2
0237+040	02:39:51.26314(7)	+04:16:21.4097(22)	-0.1(5.7)	-0.7(6.6)	0.2(5.5)	-1.4(6.2)	1.4	1.0
0237-233	02:40:08.17429(1)	-23:09:15.7297(2)	-69.6(53.8)	-73.2(48.3)	-125.8(39.0)	-39.5(30.6)	8.4	4.2
0239+175	02:42:24.26755(205)	+17:42:58.8545(125)	-24.3(9.3)	25.4(16.6)	-24.0(9.8)	24.2(18.1)	0.4	0.4
0241+622	02:44:57.69669(3)	+62:28:06.5155(2)	8.2(42.4)	6.7(47.4)	7.7(36.2)	8.3(35.4)	1.3	0.7
0248+430	02:51:34.53669(3)	+43:15:15.8298(3)	-11.3(9.7)	25.7(11.6)	-12.2(9.5)	27.3(11.8)	1.2	1.3
0252-549	02:53:29.18043(3)	-54:41:51.4363(2)	-10.3(14.5)	1.9(32.8)	2.2(11.9)	-9.9(14.6)	1.4	0.8
0256+075	02:59:27.07663(13)	+07:47:39.6427(8)	8.2(8.2)	-1.8(17.7)	10.3(8.3)	-2.0(18.0)	0.0	0.4
0256-005	02:59:28.51613(3)	-00:19:59.9752(4)	5.7(7.9)	-11.3(6.6)	5.2(8.0)	-11.2(6.5)	0.8	0.6
0300+470	03:03:35.24221(2)	+47:16:16.2753(2)	-1.5(0.8)	2.1(1.0)	-1.5(0.8)	2.3(1.0)	0.4	0.9
0302-623	03:03:50.63150(5)	-62:11:25.5495(4)	14.5(5.8)	2.2(5.0)	15.0(5.6)	2.0(4.9)	2.8	1.2
NGC1218	03:08:26.22409(6)	+04:06:39.3047(23)	8.1(11.4)	-12.1(19.6)	16.6(11.7)	-10.2(18.6)	4.4	1.8
0306+102	03:09:03.62354(10)	+10:29:16.3408(11)	-4.7(5.7)	-0.9(5.2)	-4.4(6.1)	-0.2(5.4)	0.4	0.1
0308-611	03:09:56.09916(5)	-60:58:39.0565(4)	-5.9(2.3)	-12.1(3.1)	-5.8(2.5)	-12.0(3.0)	0.2	0.4
0307+380	03:10:49.88002(19)	+38:14:53.8377(11)	-6.1(5.0)	4.5(6.9)	-6.1(4.8)	5.0(6.9)	0.5	0.2
0309+411	03:13:01.96197(6)	+41:20:01.1845(5)	-7.6(4.2)	-10.1(5.9)	-7.9(4.0)	-9.8(6.1)	2.5	2.3
0319+121	03:21:53.10391(165)	+12:21:13.9545(69)	5.2(3.1)	-14.9(20.3)	4.9(3.4)	-14.8(21.8)	0.2	0.1
0322+222	03:25:36.81400(34)	+22:24:00.3675(20)	-4.4(3.1)	6.8(2.6)	-4.6(3.2)	7.0(2.4)	1.0	0.9
0325+395	03:28:50.31210(2)	+39:40:44.5665(2)	6.5(39.1)	-22.7(45.2)	6.1(36.9)	-25.1(43.4)	0.7	1.3
0326+278	03:29:57.66941(3)	+27:56:15.4995(2)	-13.2(51.1)	-15.2(18.2)	-14.5(36.5)	8.1(9.9)	0.2	3.2
0332-403	03:34:13.65446(2)	-40:08:25.3978(3)	-0.5(4.2)	17.1(4.6)	-0.7(4.1)	17.6(5.0)	2.2	0.5
0334-546	03:35:53.92448(46)	-54:30:25.1169(28)	11.5(8.7)	10.2(18.2)	12.0(8.4)	8.2(17.8)	0.8	0.7
NRAO140	03:36:30.10753(5)	+32:18:29.3420(4)	-2.2(4.7)	-9.3(4.7)	-3.1(4.9)	-9.1(4.9)	1.5	0.2
0335-364	03:36:54.02355(2)	-36:16:06.2237(3)	-43.6(35.1)	28.8(30.2)	-30.7(29.8)	32.1(27.8)	4.5	1.2
CTA26	03:39:30.93779(2)	-01:46:35.8041(1)	1.1(1.3)	-1.7(0.8)	1.2(1.2)	-1.7(0.9)	0.2	0.7
0338-214	03:40:35.60782(3)	-21:19:31.1729(4)	-7.2(5.4)	1.8(6.5)	-7.5(5.4)	1.4(6.2)	1.5	2.1
0341+158	03:44:23.17230(36)	+15:59:43.3683(18)	-8.5(12.8)	1.6(31.2)	-8.2(13.0)	1.5(17.7)	0.4	0.5
0346-279	03:48:38.14460(3)	-27:49:13.5657(6)	-9.2(7.9)	-28.0(13.2)	-9.2(8.0)	-29.4(12.8)	1.1	0.4
0345+460	03:49:18.74144(7)	+46:09:59.6569(5)	4.4(3.5)	-3.5(4.8)	3.8(4.0)	-3.4(4.7)	2.0	1.8
0347-211	03:49:57.82669(8)	-21:02:47.7412(12)	-0.3(5.2)	-8.1(6.2)	-0.7(5.2)	-7.4(6.2)	0.2	0.3
NRAO150	03:59:29.74713(11)	+50:57:50.1616(5)	6.2(2.0)	16.6(2.2)	6.0(1.9)	16.6(2.3)	1.3	0.8

Table 7 continued

Table 7 (*continued*)

Name	Gaia 2015.0 Coordinates		VLBA PM		VLBA+Gaia PM		Gaia-VLBA Offset	
	RA (J2000)	Dec (J2000)	μ_α	μ_δ	μ_α	μ_δ	$\Delta\alpha$	$\Delta\delta$
			(h:m:s)	(d:m:s)	(mas yr $^{-1}$)	(mas yr $^{-1}$)	(σ)	(σ)
0358+210	04:01:45.16650(22)	+21:10:28.5875(5)	5.5(6.7)	0.7(9.5)	4.8(6.6)	0.1(9.3)	1.9	1.0
0400-319	04:02:21.26593(7)	-31:47:25.9488(16)	-27.3(11.3)	10.1(14.9)	-28.3(12.4)	7.1(15.7)	0.9	2.1
0402-362	04:03:53.74991(2)	-36:05:01.9132(2)	5.3(2.6)	6.4(3.6)	5.3(2.7)	6.8(3.7)	0.3	0.2
0403-132	04:05:34.00338(2)	-13:08:13.6910(2)	0.8(3.9)	-7.5(7.0)	0.7(3.8)	-8.0(7.3)	0.6	0.2
0405-385	04:06:59.03530(2)	-38:26:28.0416(3)	10.1(4.2)	22.6(7.5)	10.2(4.0)	23.2(7.2)	1.8	1.9
0405-123	04:07:48.43098(1)	-12:11:36.6598(1)	-9.1(10.9)	25.3(22.2)	-7.3(9.9)	3.5(16.9)	0.1	3.3
0406-127	04:09:05.76974(3)	-12:38:48.1441(3)	12.6(6.3)	2.0(11.8)	12.4(6.0)	1.0(11.5)	0.1	0.9
0406+121	04:09:22.00882(8)	+12:17:39.8478(6)	-28.1(17.8)	47.2(28.8)	-25.2(19.6)	42.5(28.0)	1.7	0.7
0409+229	04:12:43.66687(4)	+23:05:05.4524(3)	6.6(12.7)	3.0(15.6)	7.1(10.9)	-2.2(10.6)	0.1	0.9
0414-189	04:16:36.54440(5)	-18:51:08.3397(7)	0.9(4.4)	9.7(5.8)	1.3(4.6)	9.4(5.7)	0.9	0.7
0420+022	04:22:52.21462(11)	+02:19:26.9309(10)	2.6(5.1)	-11.8(7.6)	2.9(5.1)	-12.1(7.1)	0.3	0.1
0420-014	04:23:15.80068(4)	-01:20:33.0649(5)	-5.5(0.6)	-8.5(0.8)	-5.5(0.7)	-8.5(0.9)	1.0	1.3
0420+417	04:23:56.00974(6)	+41:50:02.7132(3)	2.9(10.2)	9.0(6.5)	3.2(10.0)	10.0(6.3)	0.9	0.6
0422-380	04:24:42.24374(4)	-37:56:20.7834(8)	-0.1(7.5)	2.0(8.0)	-0.9(7.7)	2.0(8.3)	1.0	1.2
0422+004	04:24:46.84206(1)	+00:36:06.3292(1)	2.2(4.4)	16.9(8.4)	2.5(4.6)	15.7(8.2)	0.0	2.0
0423+051	04:26:36.60408(4)	+05:18:19.8721(5)	-17.2(24.3)	42.0(19.5)	-19.0(20.2)	24.3(12.7)	0.5	1.2
0426-380	04:28:40.42425(2)	-37:56:19.5806(2)	-5.8(8.2)	-12.1(8.6)	-7.2(8.4)	-11.0(8.7)	1.2	0.3
0426+273	04:29:52.96070(16)	+27:24:37.8763(13)	-2.5(2.8)	-21.2(6.1)	-2.5(2.5)	-20.4(6.2)	0.4	0.2
0430+289	04:33:37.82984(10)	+29:05:55.4758(26)	2.1(2.7)	7.9(2.9)	2.4(2.8)	8.1(3.1)	0.2	0.5
0434-188	04:37:01.48272(3)	-18:44:48.6137(4)	0.9(5.2)	6.7(14.5)	0.3(4.9)	6.1(13.6)	0.6	0.7
0436-129	04:38:35.02097(6)	-12:51:03.3587(7)	3.1(8.0)	17.5(13.6)	2.6(8.2)	19.0(14.7)	0.7	0.4
0437-454	04:39:00.85465(6)	-45:22:22.5629(8)	-11.7(9.5)	5.6(10.9)	-11.6(9.6)	5.3(10.5)	0.3	0.3
NRAO190	04:42:38.66077(5)	-00:17:43.4202(6)	-21.3(10.6)	-29.1(4.3)	-20.6(9.9)	-28.6(3.3)	0.9	1.4
0442+389	04:46:11.49410(9)	+39:00:17.0996(7)	-0.3(15.5)	-28.2(25.5)	-0.9(16.5)	-29.8(24.4)	0.8	0.2
0446+112	04:49:07.67104(10)	+11:21:28.5964(7)	9.0(4.0)	-5.3(5.0)	9.3(3.9)	-5.1(4.7)	0.6	0.0
0444+634	04:49:23.31072(25)	+63:32:09.4338(16)	8.1(22.1)	3.2(28.1)	8.5(20.1)	3.2(20.6)	0.5	0.2
0454-810	04:50:05.44056(79)	-81:01:02.2362(194)	1.0(5.8)	-2.7(6.2)	0.7(5.8)	-3.1(6.5)	0.5	0.2
0454-463	04:55:50.77252(2)	-46:15:58.6798(3)	-9.4(19.2)	40.1(17.7)	-10.6(19.6)	40.2(18.8)	1.6	0.2
0454-234	04:57:03.17921(1)	-23:24:52.0203(2)	-3.7(0.7)	-7.0(0.8)	-3.8(0.7)	-7.1(0.8)	1.9	0.1
0457+024	04:59:52.05069(3)	+02:29:31.1766(4)	13.0(11.0)	42.4(10.3)	12.5(10.8)	39.5(9.0)	0.3	1.3
0458-020	05:01:12.80986(7)	-01:59:14.2569(9)	-2.5(0.9)	-10.4(0.8)	-2.5(0.9)	-10.4(0.8)	0.4	0.5
0459+060	05:02:15.44587(4)	+06:09:07.4937(3)	-49.3(23.8)	-52.3(30.9)	-48.7(11.6)	-48.1(9.4)	0.1	1.0
0459+135	05:02:33.21956(6)	+13:38:10.9584(9)	0.8(8.1)	-0.9(12.6)	0.3(6.0)	0.2(9.4)	0.7	0.5
0502+049	05:05:23.18473(2)	+04:59:42.7244(2)	-4.7(15.7)	-15.0(17.8)	-3.7(13.8)	-14.9(11.4)	0.6	0.4
0506-612	05:06:43.98872(4)	-61:09:40.9935(3)	17.3(6.5)	-17.9(9.8)	16.8(7.0)	-15.3(10.5)	0.8	1.4
0454+844	05:08:42.36318(54)	+84:32:04.5439(8)	6.2(4.8)	19.7(3.2)	6.9(4.7)	19.7(3.0)	0.6	0.5
0506+101	05:09:27.45722(7)	+10:11:44.5991(10)	-11.1(5.0)	18.4(7.9)	-10.7(4.8)	18.8(8.0)	2.1	1.1
0507+179	05:10:02.36911(3)	+18:00:41.5819(3)	1.4(3.5)	-4.2(5.4)	1.0(3.4)	-2.6(4.9)	0.8	1.3
0508+138	05:11:38.31969(5)	+13:57:19.1945(10)	13.5(17.1)	-21.8(15.3)	15.1(15.2)	-20.5(16.7)	0.2	1.3
0511-220	05:13:49.11430(10)	-21:59:16.0896(35)	-5.2(10.2)	19.2(17.7)	-5.4(9.4)	21.0(19.1)	0.2	0.7
0516-621	05:16:44.92615(4)	-62:07:05.3895(3)	-1.2(6.6)	-10.7(7.7)	-1.0(6.6)	-10.6(7.4)	0.4	0.4
3C138	05:21:09.88580(3)	+16:38:22.0524(5)	164.1(87.1)	-66.5(43.2)	119.7(81.8)	-52.4(39.0)	7.5	1.9
0522-611	05:22:34.42550(5)	-61:07:57.1333(5)	0.8(10.1)	3.0(11.4)	0.4(10.1)	3.8(10.9)	0.5	0.8
0521-365	05:22:57.98439(2)	-36:27:30.8491(2)	-8.5(5.4)	9.7(7.6)	-8.3(5.1)	10.5(7.3)	15.2	9.3
0524-460	05:25:31.40014(2)	-45:57:54.6850(2)	34.6(35.2)	63.7(28.9)	10.3(17.6)	29.7(16.0)	2.3	2.9
0524-485	05:26:16.67140(3)	-48:30:36.7923(5)	11.4(13.2)	1.2(21.7)	12.3(13.7)	-3.6(21.1)	2.3	0.8
0524+034	05:27:32.70543(4)	+03:31:31.5153(11)	1.6(7.5)	-4.9(11.3)	0.6(7.6)	-4.3(11.8)	0.2	1.2

Table 7 continued

Table 7 (continued)

Name	Gaia 2015.0 Coordinates		VLBA PM		VLBA+Gaia PM		Gaia-VLBA Offset	
	RA (J2000) (h:m:s)	Dec (J2000) (d:m:s)	μ_α	μ_δ	μ_α	μ_δ	$\Delta\alpha$	$\Delta\delta$
			(μ as yr $^{-1}$)	(σ)	(σ)			
0530-727	05:29:30.04209(29)	-72:45:28.5074(9)	-6.0(4.1)	-6.1(4.9)	-5.6(4.0)	-6.1(4.6)	0.3	0.0
0528-250	05:30:07.96279(1)	-25:03:29.8992(3)	-9.7(7.3)	0.7(10.3)	-9.6(7.3)	1.7(10.2)	0.4	0.8
0529+075	05:32:38.99848(4)	+07:32:43.3448(7)	3.0(140.2)	14.4(82.4)	5.1(38.2)	-19.4(33.2)	0.0	1.8
0529+483	05:33:15.86593(9)	+48:22:52.8076(7)	-1.6(3.0)	14.8(4.0)	-1.8(2.9)	15.0(4.0)	1.5	0.2
0534-611	05:34:35.77248(12)	-61:06:07.0727(7)	1.0(12.7)	-23.2(12.0)	0.5(12.7)	-23.1(11.8)	0.2	0.9
0534-340	05:36:28.43233(2)	-34:01:11.4682(5)	-16.2(15.2)	50.0(18.5)	-16.3(16.2)	50.2(18.8)	1.1	0.2
0537-441	05:38:50.36155(2)	-44:05:08.9389(3)	5.8(1.3)	7.6(1.5)	5.9(1.3)	7.3(1.5)	0.4	0.1
0537-158	05:39:32.01013(2)	-15:50:30.3208(3)	23.9(33.7)	59.9(72.8)	0.0(8.8)	38.7(13.6)	1.9	1.5
0536+145	05:39:42.36566(32)	+14:33:45.5651(36)	-1.6(4.6)	4.6(4.9)	-1.8(4.1)	4.8(4.7)	1.0	1.0
0537-286	05:39:54.28150(3)	-28:39:55.9480(5)	11.7(7.3)	-11.3(5.4)	11.7(7.6)	-11.5(5.5)	0.8	0.3
0539-057	05:41:38.08282(51)	-05:41:49.3107(932)	-1.3(15.6)	-16.6(26.9)	0.7(15.5)	-17.0(26.2)	1.1	1.3
3C147	05:42:36.13805(4)	+49:51:07.2348(4)	-0.4(12.5)	-4.2(8.4)	2.6(9.2)	-0.9(8.8)	4.1	2.8
0549-575	05:50:09.58023(6)	-57:32:24.3975(6)	0.6(13.2)	32.5(16.7)	1.0(12.7)	30.7(17.1)	0.5	1.8
0548+378	05:52:17.93683(44)	+37:54:25.2839(44)	-21.4(13.8)	9.6(12.8)	-19.9(14.5)	8.4(12.7)	0.2	0.3
0552+398	05:55:30.80563(3)	+39:48:49.1651(4)	0.2(0.4)	-3.4(0.4)	0.2(0.4)	-3.5(0.4)	0.6	0.3
0554+242	05:57:04.71353(22)	+24:13:55.2979(39)	5.9(26.7)	30.3(28.6)	6.3(22.4)	28.6(24.5)	0.3	0.3
0601+245	06:04:55.12144(20)	+24:29:55.0255(170)	42.1(70.3)	17.5(32.2)	42.4(72.2)	18.0(45.8)	0.1	0.7
0602+673	06:07:52.67154(7)	+67:20:55.4096(6)	0.5(0.8)	20.4(1.2)	0.5(0.8)	20.4(1.2)	1.0	0.9
0605-085	06:07:59.69926(3)	-08:34:49.9785(8)	-10.3(10.5)	11.2(8.4)	-8.8(9.9)	10.9(7.9)	1.2	0.5
0610+260	06:13:50.13916(6)	+26:04:36.7139(62)	-74.1(35.3)	30.7(20.7)	-69.5(24.8)	29.6(22.9)	0.9	1.0
0611+131	06:13:57.69279(5)	+13:06:45.4006(6)	-0.4(9.7)	17.3(21.5)	0.8(8.6)	14.0(18.1)	0.6	0.5
0609+607	06:14:23.86617(8)	+60:46:21.7554(6)	0.3(6.0)	-0.7(9.0)	0.3(5.9)	-0.2(9.3)	0.2	0.8
0613+570	06:17:16.92263(9)	+57:01:16.4259(25)	7.8(7.3)	-11.6(7.4)	7.6(6.8)	-12.0(6.6)	0.7	1.1
0620+389	06:24:19.02159(55)	+38:56:48.7321(68)	-24.7(14.9)	15.9(15.9)	-24.9(14.2)	16.4(15.0)	0.6	0.6
0615+820	06:26:03.00613(15)	+82:02:25.5675(3)	15.2(9.6)	-18.6(11.9)	14.0(9.0)	-20.5(11.6)	1.3	0.9
0627-199	06:29:23.76195(9)	-19:59:19.7237(8)	-7.5(8.5)	-2.6(8.2)	-7.5(9.3)	-2.8(8.2)	0.9	0.0
0629-418	06:31:11.99809(5)	-41:54:26.9467(8)	13.4(26.5)	71.1(59.9)	17.2(20.1)	63.0(49.6)	0.9	1.4
0632-235	06:34:59.00107(8)	-23:35:11.9583(18)	17.1(17.5)	-4.4(14.3)	20.0(16.8)	-4.2(14.9)	0.7	0.5
0636+680	06:42:04.25736(2)	+67:58:35.6214(2)	-7.6(6.1)	2.5(4.1)	-8.4(5.8)	3.7(3.9)	1.6	2.8
0646-306	06:48:14.09651(7)	-30:44:19.6601(11)	-4.6(8.4)	14.6(7.4)	-4.1(8.1)	14.2(7.5)	0.8	0.4
0656+082	06:59:17.99606(3)	+08:13:30.9526(5)	-7.5(2.8)	18.0(5.0)	-7.3(2.9)	18.1(5.3)	1.1	1.8
0657+172	07:00:01.52555(4)	+17:09:21.7003(8)	7.3(1.4)	-5.2(1.8)	7.2(1.4)	-5.4(1.9)	0.2	1.4
0700-197	07:02:42.90066(1)	-19:51:22.0354(3)	-22.0(6.0)	8.2(14.0)	-22.1(5.7)	9.2(13.5)	0.1	0.4
0714+457	07:17:51.85249(8)	+45:38:03.2599(8)	16.0(9.5)	-33.0(7.6)	16.3(9.0)	-32.5(8.2)	0.7	1.0
0716+714	07:21:53.44853(2)	+71:20:36.3633(2)	3.7(1.5)	0.8(2.1)	3.7(1.6)	0.6(2.1)	2.3	0.8
0722+145	07:25:16.80778(3)	+14:25:13.7458(5)	5.3(3.4)	-3.6(4.6)	5.1(3.1)	-3.7(5.1)	0.5	1.6
0723-008	07:25:50.63994(4)	-00:54:56.5442(6)	-50.8(6.3)	108.1(13.7)	-50.0(6.5)	107.5(13.1)	0.7	2.5
0723+219	07:26:14.26075(5)	+21:53:20.1133(7)	13.4(7.4)	-34.1(11.0)	14.6(6.8)	-33.1(10.2)	0.2	0.9
0727-115	07:30:19.11244(5)	-11:41:12.6001(6)	0.3(0.5)	-2.2(0.6)	0.3(0.5)	-2.3(0.6)	0.6	1.0
0729+259	07:32:56.27518(5)	+25:48:38.7961(11)	2.3(5.7)	17.0(9.5)	2.1(5.9)	15.7(9.1)	1.7	0.4
0735+178	07:38:07.39375(2)	+17:42:18.9983(3)	-12.8(4.0)	4.9(3.0)	-12.4(3.5)	5.0(2.8)	1.0	0.3
0738-674	07:38:56.49653(17)	-67:35:50.8248(20)	-21.4(17.2)	-52.0(32.7)	-15.0(17.2)	-52.4(34.6)	2.1	0.9
0736+017	07:39:18.03389(2)	+01:37:04.6176(2)	-0.5(4.2)	-0.6(3.0)	-0.1(4.0)	-0.7(3.0)	0.1	0.4
0738+491	07:42:02.74931(28)	+49:00:15.6104(15)	6.6(3.6)	-2.6(3.5)	6.5(3.7)	-2.7(3.7)	1.3	1.0
0743-006	07:45:54.08227(2)	-00:44:17.5404(2)	7.7(4.2)	10.8(6.9)	7.6(4.0)	9.5(6.7)	3.0	3.5
0743+259	07:46:25.87432(17)	+25:49:02.1336(8)	-3.6(2.8)	-32.8(3.8)	-3.5(2.8)	-33.4(3.6)	0.8	1.0
0743+277	07:46:40.43243(53)	+27:34:59.0503(88)	2.4(5.9)	-13.3(6.6)	2.3(6.0)	-13.0(6.3)	0.2	0.4

Table 7 continued

Table 7 (*continued*)

Name	Gaia 2015.0 Coordinates		VLBA PM		VLBA+Gaia PM		Gaia-VLBA Offset	
	RA (J2000)	Dec (J2000)	μ_α	μ_δ	μ_α	μ_δ	$\Delta\alpha$	$\Delta\delta$
			(h:m:s)	(d:m:s)	(mas yr $^{-1}$)	(mas yr $^{-1}$)	(σ)	(σ)
0745+241	07:48:36.10923(3)	+24:00:24.1102(2)	3.1(3.3)	-0.5(3.0)	2.4(3.2)	-0.3(2.9)	1.8	1.3
0747+185	07:50:00.32996(8)	+18:23:11.4068(5)	2.4(8.7)	0.2(11.1)	3.0(8.5)	-0.6(12.6)	0.1	0.7
0748+126	07:50:52.04574(2)	+12:31:04.8282(1)	13.9(3.0)	4.9(2.0)	13.9(2.8)	5.3(2.0)	0.1	0.1
0749+540	07:53:01.38464(4)	+53:52:59.6379(4)	0.4(0.8)	3.0(0.7)	0.4(0.8)	3.0(0.8)	1.7	2.0
0754+100	07:57:06.64298(2)	+09:56:34.8525(1)	-2.6(5.2)	-7.6(11.4)	-1.6(5.3)	-2.2(10.1)	1.5	2.3
0759+183	08:02:48.03194(15)	+18:09:49.2496(10)	20.1(5.1)	-3.5(8.7)	20.4(4.7)	-3.5(8.8)	0.2	0.3
0800+618	08:05:18.17956(10)	+61:44:23.7021(9)	9.0(3.6)	-13.5(6.1)	9.2(3.9)	-12.7(6.3)	0.0	1.8
0805+046	08:07:57.53823(4)	+04:32:34.5348(2)	-91.8(18.1)	25.4(12.5)	-94.0(18.9)	53.3(17.1)	7.8	18.3
0805-077	08:08:15.53600(4)	-07:51:09.8860(3)	-20.7(8.7)	-13.7(3.8)	-22.4(8.3)	-12.1(3.1)	0.7	2.1
0804+499	08:08:39.66630(7)	+49:50:36.5307(5)	3.7(0.7)	0.4(0.7)	3.7(0.7)	0.4(0.7)	0.1	0.6
0805+410	08:08:56.65204(4)	+40:52:44.8892(4)	5.5(1.1)	9.4(1.3)	5.4(1.1)	9.4(1.3)	0.3	0.6
0808+019	08:11:26.70724(4)	+01:46:52.2202(3)	-0.1(1.7)	-0.7(1.9)	-0.2(1.8)	-0.5(2.0)	2.0	0.1
0812+367	08:15:25.94487(4)	+36:35:15.1487(5)	5.1(4.5)	-4.7(6.2)	5.2(4.5)	-5.2(7.1)	0.0	0.2
0814+425	08:18:15.99961(3)	+42:22:45.4148(4)	5.9(2.0)	0.1(1.8)	6.0(1.9)	0.0(1.8)	0.4	0.2
0818-128	08:20:57.44776(6)	-12:58:59.1684(8)	-37.4(17.8)	31.0(15.3)	-28.4(15.8)	32.6(15.2)	2.9	0.6
0820+560	08:24:47.23637(4)	+55:52:42.6693(4)	8.4(5.3)	-9.7(4.9)	7.8(5.3)	-9.7(4.6)	0.3	0.3
0821+394	08:24:55.48381(3)	+39:16:41.9042(3)	3.0(2.2)	-0.3(3.1)	3.1(2.3)	0.1(3.3)	1.6	0.4
0821+621	08:25:38.61221(3)	+61:57:28.5793(2)	-34.0(31.3)	-6.9(11.9)	-21.2(9.2)	-6.6(8.8)	2.8	0.0
0823+033	08:25:50.33837(4)	+03:09:24.5199(6)	-0.6(1.1)	3.2(1.5)	-0.4(1.1)	3.1(1.4)	0.3	0.2
0823-223	08:26:01.57296(2)	-22:30:27.2033(2)	1.3(13.5)	16.3(16.2)	1.6(24.0)	13.3(19.3)	1.2	2.0
0827+243	08:30:52.08616(3)	+24:10:59.8207(2)	-1.7(2.2)	-2.2(2.2)	-1.4(2.1)	-2.1(2.1)	1.1	1.6
0829+046	08:31:48.87696(2)	+04:29:39.0859(2)	1.4(7.8)	26.8(8.3)	2.5(6.7)	22.2(6.9)	0.3	1.2
0828+493	08:32:23.21676(3)	+49:13:21.0383(3)	-3.0(7.5)	-0.5(11.6)	0.1(7.4)	-0.9(11.3)	1.6	0.2
0831+557	08:34:54.90457(83)	+55:34:21.0486(225)	4.0(42.4)	4.5(25.8)	3.7(44.2)	4.5(26.7)	0.7	1.0
0833+585	08:37:22.40961(4)	+58:25:01.8449(3)	-8.0(17.9)	5.7(7.7)	-10.6(17.3)	5.5(7.5)	1.1	0.3
0834+250	08:37:40.24569(3)	+24:54:23.1218(3)	2.5(4.8)	-7.1(4.7)	2.1(5.2)	-6.2(5.2)	0.0	0.8
0836+710	08:41:24.36530(3)	+70:53:42.1727(2)	9.4(6.3)	3.9(9.5)	10.1(5.7)	4.4(8.7)	0.3	1.4
0839+187	08:42:05.09413(3)	+18:35:40.9890(4)	32.6(8.1)	28.2(35.7)	28.7(8.3)	3.4(31.4)	2.3	4.6
0847-120	08:50:09.63565(3)	-12:13:35.3764(6)	11.7(8.7)	12.1(6.4)	11.8(9.0)	12.3(6.3)	0.3	0.4
0850+581	08:54:41.99638(3)	+57:57:29.9397(3)	-11.5(10.0)	-5.8(16.6)	-12.9(8.7)	1.6(13.8)	0.5	2.6
OJ287	08:54:48.87493(2)	+20:06:30.6408(2)	-1.5(0.4)	0.5(0.4)	-1.5(0.4)	0.5(0.4)	0.1	0.3
0854-108	08:56:41.80412(3)	-11:05:14.4306(3)	11.6(9.0)	11.7(8.5)	11.6(8.7)	10.4(8.2)	1.4	0.9
0859-140	09:02:16.83092(2)	-14:15:30.8762(3)	1.4(7.9)	20.3(26.2)	2.2(7.6)	9.4(24.4)	0.2	3.4
0859+470	09:03:03.99017(7)	+46:51:04.1393(11)	-1.2(7.4)	-0.3(5.4)	-0.7(6.9)	0.4(5.6)	1.0	1.7
0906+015	09:09:10.09161(2)	+01:21:35.6176(3)	12.8(7.6)	11.4(10.7)	12.7(7.4)	12.1(11.5)	0.8	0.1
0912+029	09:14:37.91340(7)	+02:45:59.2486(11)	4.0(3.3)	-14.0(9.7)	4.0(3.2)	-13.4(9.7)	0.5	2.0
0912+297	09:15:52.40166(2)	+29:33:24.0426(2)	11.0(11.4)	-14.1(17.3)	10.7(11.9)	-17.8(18.5)	0.5	0.6
0917+449	09:20:58.45849(2)	+44:41:53.9850(3)	7.0(6.8)	5.5(10.2)	7.1(6.1)	3.8(9.5)	0.1	0.6
0917+624	09:21:36.23104(5)	+62:15:52.1804(5)	-5.0(5.1)	11.3(4.2)	-4.8(4.9)	11.7(4.5)	0.4	0.3
0920-397	09:22:46.41827(2)	-39:59:35.0684(3)	2.7(3.6)	31.2(9.8)	2.8(3.5)	29.9(8.9)	0.3	1.1
0925-203	09:27:51.82434(2)	-20:34:51.2327(3)	3.9(7.1)	-3.8(8.5)	4.3(6.6)	-3.9(8.4)	0.9	0.4
0943+105	09:46:35.06991(6)	+10:17:06.1342(8)	23.9(12.5)	45.0(27.0)	22.9(12.1)	47.4(24.0)	0.8	0.5
0945+408	09:48:55.33812(3)	+40:39:44.5872(6)	-16.3(17.4)	-9.2(8.7)	-15.9(17.0)	-9.2(8.7)	0.7	0.7
0949+354	09:52:32.02617(5)	+35:12:52.4025(4)	-11.8(7.0)	8.4(12.1)	-11.7(7.1)	8.2(12.3)	0.0	1.3
0952+179	09:54:56.82362(3)	+17:43:31.2219(4)	-6.2(6.1)	41.9(12.8)	-5.8(6.0)	41.0(12.3)	0.4	1.6
M81	09:55:33.17361(22)	+69:03:55.0630(14)	3.1(8.0)	-20.6(4.3)	4.9(7.6)	-19.8(4.8)	2.4	1.8
0955+476	09:58:19.67166(2)	+47:25:07.8426(3)	0.4(0.6)	-0.5(0.4)	0.4(0.5)	-0.5(0.4)	0.6	0.6

Table 7 continued

Table 7 (*continued*)

Name	Gaia 2015.0 Coordinates		VLBA PM		VLBA+Gaia PM		Gaia-VLBA Offset	
	RA (J2000) (h:m:s)	Dec (J2000) (d:m:s)	μ_α	μ_δ	μ_α	μ_δ	$\Delta\alpha$	$\Delta\delta$
			(μ as yr $^{-1}$)	(σ)	(σ)			
0955+326	09:58:20.94966(2)	+32:24:02.2092(2)	1.8(3.2)	0.4(5.7)	1.6(3.0)	1.0(5.3)	1.2	1.4
0954+658	09:58:47.24512(3)	+65:33:54.8183(3)	-1.7(1.4)	-0.1(1.5)	-1.7(1.4)	-0.3(1.6)	0.5	0.9
1004-500	10:06:14.00946(18)	-50:18:13.4711(14)	-8.6(11.9)	-9.4(21.8)	-7.4(11.7)	-10.5(22.8)	0.8	0.3
1011+250	10:13:53.42879(2)	+24:49:16.4410(3)	-10.5(9.2)	-19.5(6.9)	-8.5(7.6)	-16.6(6.2)	1.2	1.7
1012+232	10:14:47.06552(3)	+23:01:16.5703(6)	11.6(3.9)	-9.5(3.1)	12.1(3.8)	-9.7(3.2)	1.8	0.7
1013+127	10:15:44.02326(10)	+12:27:07.0711(14)	-9.9(16.6)	8.0(28.5)	-10.4(15.6)	8.4(25.6)	1.3	0.6
1013+054	10:16:03.13650(17)	+05:13:02.3415(19)	19.1(8.4)	22.8(13.8)	18.4(8.1)	22.7(13.0)	0.1	0.0
1014+615	10:17:25.88733(5)	+61:16:27.4958(5)	-13.5(4.0)	-9.6(3.1)	-14.0(3.8)	-9.6(3.1)	4.6	1.4
1015+359	10:18:10.98809(3)	+35:42:39.4407(3)	5.3(6.5)	40.7(14.5)	5.1(6.4)	40.3(15.9)	0.4	0.8
1020+400	10:23:11.56565(17)	+39:48:15.3855(32)	-2.9(6.1)	8.9(7.2)	-2.2(5.7)	7.5(6.9)	0.0	0.0
1022+194	10:24:44.80957(4)	+19:12:20.4153(6)	-2.1(4.4)	1.3(4.0)	-1.8(4.3)	0.9(4.0)	0.5	0.4
1027-186	10:29:33.09772(4)	-18:52:50.2892(7)	-7.2(16.3)	10.0(40.4)	-7.1(14.0)	12.3(37.3)	0.7	0.4
1030+415	10:33:03.70785(6)	+41:16:06.2330(4)	-8.3(3.7)	8.5(4.2)	-7.9(3.6)	8.4(4.0)	0.4	0.3
1030+074	10:33:34.02446(13)	+07:11:26.1470(27)	4.5(8.2)	-12.3(6.3)	5.1(8.7)	-12.7(7.0)	1.3	0.2
1032-199	10:35:02.15526(6)	-20:11:34.3580(6)	20.9(6.0)	2.8(13.4)	20.5(6.3)	4.4(13.9)	1.0	2.4
1034-374	10:36:53.43959(4)	-37:44:15.0659(4)	-11.7(18.6)	53.4(23.8)	-14.2(19.6)	52.4(24.7)	0.4	0.4
1034-293	10:37:16.07976(2)	-29:34:02.8138(4)	7.0(2.0)	-8.8(2.4)	6.8(2.0)	-8.7(2.3)	0.7	0.7
1038+064	10:41:17.16249(3)	+06:10:16.9235(4)	-14.7(3.4)	62.0(8.1)	-15.1(3.5)	61.6(8.4)	0.1	2.1
1038+52A	10:41:46.78166(1)	+52:33:28.2310(2)	8.3(2.0)	42.5(3.2)	8.1(2.1)	42.0(3.3)	0.2	4.7
1038+52B	10:41:48.89755(2)	+52:33:55.6087(3)	3.1(346.7)	-23.8(493.5)	-49.7(14.8)	2.9(16.7)	7.8	3.0
3C245	10:42:44.60526(2)	+12:03:31.2640(4)	34.2(28.2)	-37.8(30.2)	32.6(21.4)	-32.0(19.4)	0.5	1.9
1040+244	10:43:09.03577(4)	+24:08:35.4095(5)	9.6(5.3)	13.6(7.7)	9.7(6.2)	15.0(7.7)	0.2	0.1
1039+811	10:44:23.06265(11)	+80:54:39.4434(3)	4.1(5.2)	3.0(2.7)	4.0(4.7)	3.0(2.2)	0.7	0.9
1042+071	10:44:55.91142(16)	+06:55:38.2600(23)	4.0(14.2)	-8.5(13.9)	5.7(14.6)	-8.8(12.3)	1.1	1.1
1045-188	10:48:06.62065(8)	-19:09:35.7271(6)	22.1(4.3)	-74.2(10.5)	22.3(4.3)	-73.5(10.4)	0.3	0.5
1048-313	10:51:04.77744(9)	-31:38:14.3064(10)	36.0(35.0)	37.8(35.5)	24.9(31.5)	39.8(29.4)	1.4	1.1
1049+215	10:51:48.78903(7)	+21:19:52.3135(11)	-4.8(10.8)	12.2(6.3)	-3.5(9.8)	12.0(6.1)	0.6	0.3
1053+704	10:56:53.61757(11)	+70:11:45.9156(6)	-4.0(3.5)	-6.4(2.9)	-4.0(3.5)	-6.5(2.8)	0.6	0.1
1053+815	10:58:11.53555(15)	+81:14:32.6753(3)	-7.2(1.4)	1.7(1.6)	-7.1(1.4)	1.8(1.5)	1.4	0.6
1055+018	10:58:29.60518(2)	+01:33:58.8238(2)	-2.1(2.0)	6.4(2.6)	-2.3(1.9)	6.4(2.6)	1.9	0.1
1057-797	10:58:43.30992(23)	-80:03:54.1599(5)	0.5(1.4)	-7.7(1.2)	0.5(1.3)	-7.5(1.2)	0.6	0.1
1056+212	10:59:39.04277(10)	+20:57:21.9567(11)	-11.3(6.3)	27.3(35.8)	-11.1(8.5)	30.4(36.0)	0.9	0.4
1059+282	11:02:14.28843(4)	+27:57:08.6900(7)	3.1(15.3)	3.6(11.7)	3.7(15.6)	4.5(12.4)	0.6	0.7
1100+122	11:03:03.52982(4)	+11:58:16.5979(938)	-11.5(49.5)	57.8(29.1)	-11.1(48.3)	57.4(27.7)	0.4	0.3
1101-536	11:03:52.22170(5)	-53:57:00.6979(3)	3.5(4.1)	-2.3(6.6)	3.6(4.1)	-5.8(6.9)	0.3	3.7
1101+384	11:04:27.31395(2)	+38:12:31.7987(3)	2.1(1.3)	-4.8(1.6)	2.1(1.3)	-5.1(1.7)	0.1	0.9
1104-445	11:07:08.69412(2)	-44:49:07.6179(2)	-20.1(3.2)	12.4(3.2)	-20.1(3.0)	12.4(3.2)	0.7	1.8
1105-680	11:07:12.69548(6)	-68:20:50.7260(3)	392.6(245.8)	101.3(116.0)	303.9(69.9)	142.4(39.6)	2.8	0.9
1104+728	11:07:41.72255(8)	+72:32:36.0049(4)	-13.6(9.3)	12.3(17.5)	-13.4(8.2)	12.8(15.8)	0.2	0.4
1111+149	11:13:58.69510(2)	+14:42:26.9514(7)	-5.2(5.9)	8.5(6.7)	-5.4(6.5)	8.2(6.6)	0.7	1.9
1116-462	11:18:26.95763(2)	-46:34:15.0018(2)	36.0(49.9)	5.6(64.3)	-4.2(25.7)	-23.1(15.8)	3.5	2.5
1116+128	11:18:57.30153(5)	+12:34:41.7126(40)	-2.9(14.3)	-3.6(20.0)	0.4(14.4)	-4.4(19.4)	1.9	1.3
1123+264	11:25:53.71192(3)	+26:10:19.9783(7)	-8.4(2.6)	7.2(2.5)	-8.3(2.6)	7.5(2.7)	0.0	0.7
1124-186	11:27:04.39249(3)	-18:57:17.4423(2)	1.8(1.2)	-6.8(1.1)	1.7(1.1)	-6.8(1.2)	1.2	1.9
1125+366	11:27:58.87085(7)	+36:20:28.3512(7)	7.2(18.7)	-0.4(28.6)	6.4(19.2)	-0.8(30.5)	0.3	0.1
1127-145	11:30:07.05254(2)	-14:49:27.3881(2)	3.6(25.1)	-4.8(18.1)	-12.5(15.8)	5.6(11.1)	2.0	1.9
1128+385	11:30:53.28261(4)	+38:15:18.5469(8)	-2.4(0.6)	1.8(0.8)	-2.4(0.6)	1.7(0.7)	0.0	0.1

Table 7 continued

Table 7 (*continued*)

Name	Gaia 2015.0 Coordinates		VLBA PM		VLBA+Gaia PM		Gaia-VLBA Offset	
	RA (J2000)	Dec (J2000)	μ_α	μ_δ	μ_α	μ_δ	$\Delta\alpha$	$\Delta\delta$
			(h:m:s)	(d:m:s)	(mas yr $^{-1}$)	(mas yr $^{-1}$)	(σ)	(σ)
1128-047	11:31:30.51688(43)	-05:00:19.6629(37)	14.9(21.7)	25.4(15.5)	13.8(18.3)	25.0(20.0)	0.3	1.6
1130+009	11:33:20.05568(9)	+00:40:52.8385(7)	-10.0(6.4)	-4.5(8.8)	-10.3(6.8)	-2.7(9.2)	1.2	1.9
1133-032	11:36:24.57694(6)	-03:30:29.4953(5)	6.5(4.9)	-0.0(6.9)	7.1(5.3)	-0.3(7.4)	0.0	2.9
MRK180	11:36:26.40861(5)	+70:09:27.3073(3)	11.9(100.1)	6.9(58.5)	21.3(24.7)	7.3(13.9)	3.1	0.9
NGC3862	11:45:05.00908(7)	+19:36:22.7478(9)	-12.9(29.1)	-61.0(38.8)	-9.2(16.3)	48.5(88.7)	0.7	8.2
1143-696	11:45:53.62417(5)	-69:54:01.7978(2)	27.7(9.4)	29.1(13.2)	27.7(8.5)	26.2(12.3)	0.2	1.3
1143-245	11:46:08.10341(2)	-24:47:32.9014(1)	13.0(16.5)	45.6(18.5)	26.5(16.2)	-183.5(50.8)	3.9	37.3
1143-287	11:46:26.18860(6)	-28:59:18.5057(7)	-56.7(82.5)	-25.9(69.0)	-47.2(61.2)	-50.8(37.3)	1.1	1.3
1144+402	11:46:58.29795(2)	+39:58:34.3045(2)	-2.4(1.6)	-2.3(2.2)	-2.2(1.8)	-2.3(2.3)	1.5	0.4
1144-379	11:47:01.37074(14)	-38:12:11.0242(5)	4.0(1.6)	3.8(1.7)	3.9(1.7)	3.7(1.7)	0.2	1.6
1145-071	11:47:51.55404(3)	-07:24:41.1410(2)	4.7(4.0)	6.2(3.4)	4.7(4.0)	6.6(3.2)	0.1	0.9
1145+268	11:47:59.76393(2)	+26:35:42.3323(3)	4.7(5.9)	-35.4(10.3)	5.0(6.4)	-36.3(10.0)	1.0	0.3
1147+245	11:50:19.21216(2)	+24:17:53.8352(2)	2.2(5.0)	-0.8(4.0)	2.4(4.6)	-1.1(3.9)	1.1	0.2
1148-001	11:50:43.87084(2)	-00:23:54.2045(1)	36.6(23.1)	24.4(24.8)	44.9(14.2)	44.0(16.3)	2.5	4.2
1149-084	11:52:17.20951(5)	-08:41:03.3136(4)	7.2(6.2)	-14.3(4.0)	7.2(6.1)	-13.9(4.2)	0.0	1.0
1150+812	11:53:12.49940(16)	+80:58:29.1545(3)	-3.7(6.6)	-11.0(5.7)	-3.7(6.3)	-10.5(5.1)	1.3	0.1
1150+497	11:53:24.46665(2)	+49:31:08.8297(3)	2.9(11.0)	8.7(13.6)	5.3(10.1)	7.1(11.7)	0.9	1.6
1155+251	11:58:25.78768(9)	+24:50:17.9653(7)	19.3(34.4)	-39.5(36.2)	27.1(30.3)	5.3(23.7)	1.3	2.9
1156-094	11:59:12.71135(70)	-09:40:52.0537(24)	-42.8(39.0)	-67.5(90.7)	-41.0(38.0)	-71.9(72.9)	0.5	1.9
1156-663	11:59:18.30552(15)	-66:35:39.4270(7)	-3.3(23.6)	-4.2(37.5)	-1.2(23.5)	-6.5(35.6)	0.5	0.1
1156+295	11:59:31.83393(2)	+29:14:43.8268(1)	0.2(0.8)	4.7(1.5)	0.1(0.9)	4.9(1.5)	1.0	0.8
1212+171	12:15:03.97912(10)	+16:54:37.9582(12)	17.3(13.9)	-7.1(16.2)	17.2(14.3)	-6.6(18.1)	0.3	1.2
1213-172	12:15:46.74897(280)	-17:31:45.3597(506)	-4.5(3.4)	3.3(6.1)	-4.0(3.4)	3.6(5.5)	1.0	0.9
1213+350	12:15:55.59889(10)	+34:48:15.2023(9)	7.5(10.6)	11.5(10.4)	-1.2(11.3)	-15.8(12.9)	20.8	20.3
1215+303	12:17:52.08199(1)	+30:07:00.6356(1)	-2.4(5.2)	13.6(7.0)	-1.1(5.3)	11.8(6.8)	1.9	2.6
1219+285	12:21:31.69054(2)	+28:13:58.5001(2)	-1.4(12.3)	13.4(10.4)	3.2(10.1)	4.6(5.2)	1.6	1.3
1219+044	12:22:22.54965(3)	+04:13:15.7759(2)	6.2(1.1)	-3.5(2.0)	6.3(1.1)	-3.6(2.0)	0.9	0.4
1221+809	12:23:40.49367(17)	+80:40:04.3413(3)	0.8(2.4)	3.0(3.6)	0.5(2.4)	3.0(3.6)	0.5	2.5
1222+037	12:24:52.42197(5)	+03:30:50.2919(5)	33.6(30.1)	-7.3(32.9)	34.2(26.7)	-10.3(20.9)	0.2	1.6
1236+077	12:39:24.58835(3)	+07:30:17.1895(3)	2.8(5.0)	-4.1(6.3)	2.5(5.1)	-4.6(6.2)	0.8	1.5
1237-101	12:39:43.06157(3)	-10:23:28.6927(2)	-87.5(11.7)	24.8(12.4)	-83.9(11.2)	21.2(10.8)	5.2	1.0
1239+376	12:42:09.81239(7)	+37:20:05.6935(7)	-12.2(30.8)	-83.6(56.7)	-11.0(18.2)	-73.8(56.8)	0.2	3.2
1240+381	12:42:51.36907(3)	+37:51:00.0257(3)	0.9(12.8)	6.5(11.4)	0.9(12.6)	5.9(10.7)	0.1	1.2
1244-255	12:46:46.80204(2)	-25:47:49.2889(2)	-3.2(5.2)	-7.0(3.8)	-3.5(4.7)	-6.5(4.0)	0.1	0.4
1245-454	12:48:28.49512(3)	-45:59:47.1801(4)	-29.4(43.6)	38.4(87.7)	-23.4(26.7)	0.8(45.4)	0.5	1.9
1252+119	12:54:38.25563(2)	+11:41:05.8949(2)	6.0(8.8)	5.4(6.2)	5.8(8.6)	4.6(6.1)	1.1	0.8
1251-713	12:54:59.92150(13)	-71:38:18.4368(6)	14.3(5.3)	1.8(6.0)	14.1(5.2)	1.5(5.6)	0.0	0.4
1255-316	12:57:59.06079(3)	-31:55:16.8524(3)	13.8(2.3)	27.3(3.8)	13.7(2.5)	26.9(3.8)	1.5	3.0
1255-177	12:58:38.30186(12)	-18:00:03.1248(10)	-8.7(9.0)	35.9(10.1)	-8.5(8.7)	36.2(11.5)	1.3	0.5
1257+145	13:00:20.91884(3)	+14:17:18.5313(3)	3.6(18.6)	34.5(40.9)	7.6(15.9)	5.8(25.7)	0.5	2.4
1300+580	13:02:52.46536(13)	+57:48:37.6092(13)	5.2(0.7)	11.4(0.8)	5.2(0.7)	11.4(0.8)	0.6	0.1
1302-102	13:05:33.01500(2)	-10:33:19.4285(2)	16.8(27.4)	-9.0(34.6)	-5.7(15.8)	-20.3(12.5)	3.5	1.2
1306+360	13:08:23.70910(4)	+35:46:37.1644(3)	-9.0(4.9)	9.2(8.8)	-8.7(5.5)	10.2(9.2)	0.6	1.0
1307+121	13:09:33.93248(3)	+11:54:24.5540(3)	15.2(13.7)	35.6(32.3)	17.9(10.3)	55.0(15.7)	0.4	1.8
1308+328	13:10:59.40275(2)	+32:33:34.4495(3)	-0.2(2.7)	-3.0(2.3)	-0.1(2.6)	-2.9(2.1)	0.9	0.1
1308+554	13:11:03.21074(7)	+55:13:54.3231(5)	-25.9(24.1)	22.9(28.2)	-27.5(23.5)	23.4(25.6)	0.8	1.2
1313-333	13:16:07.98590(5)	-33:38:59.1724(6)	3.6(3.8)	-2.8(7.4)	3.4(3.7)	-2.6(7.6)	0.8	0.4

Table 7 continued

Table 7 (*continued*)

Name	Gaia 2015.0 Coordinates		VLBA PM		VLBA+Gaia PM		Gaia-VLBA Offset	
	RA (J2000) (h:m:s)	Dec (J2000) (d:m:s)	μ_α	μ_δ	μ_α	μ_δ	$\Delta\alpha$	$\Delta\delta$
			(mas yr $^{-1}$)	(σ)	(σ)			
OP326	13:17:36.49422(2)	+34:25:15.9325(2)	-5.7(12.4)	-0.5(13.2)	-2.2(10.4)	1.7(8.1)	2.0	0.3
1318+225	13:21:11.20254(3)	+22:16:12.1082(2)	-7.0(142.8)	4.1(123.8)	-8.0(8.0)	2.1(12.1)	0.4	0.9
1319-093	13:22:36.91267(7)	-09:37:37.7994(11)	-14.8(67.2)	-30.2(176.7)	-15.1(85.9)	-29.4(182.0)	0.6	1.0
1324+224	13:27:00.86129(4)	+22:10:50.1624(3)	-3.3(2.6)	-8.5(3.2)	-3.6(2.7)	-8.3(3.1)	0.7	1.4
1325-558	13:29:01.14492(3)	-56:08:02.6646(7)	7.6(21.1)	37.3(26.2)	11.0(19.8)	40.2(25.7)	0.1	1.3
1327+504	13:29:05.80264(9)	+50:09:26.4001(8)	2.2(8.4)	-7.2(12.5)	2.9(8.6)	-6.4(12.5)	0.8	0.8
3C286	13:31:08.28830(1)	+30:30:32.9621(1)	22.0(45.4)	-24.0(37.9)	158.0(34.8)	168.0(28.8)	20.5	32.2
1330+476	13:32:45.24645(5)	+47:22:22.6682(4)	7.9(8.5)	4.5(7.5)	8.5(7.9)	4.8(7.1)	0.4	0.9
1334-127	13:37:39.78280(5)	-12:57:24.6928(9)	-1.3(0.7)	-3.1(0.9)	-1.2(0.7)	-3.1(0.8)	0.4	0.7
1336-237	13:39:01.74642(4)	-24:01:14.0058(4)	31.3(119.3)	-61.6(319.7)	31.7(81.9)	-58.5(323.6)	0.2	1.4
1342+662	13:43:45.95962(15)	+66:02:25.7454(7)	-3.0(8.1)	6.2(4.6)	-3.5(8.0)	6.5(4.8)	0.3	0.4
1342+663	13:44:08.67964(9)	+66:06:11.6432(4)	-41.3(7.1)	-9.8(2.6)	-40.9(7.3)	-9.8(2.8)	0.7	1.2
1347+539	13:49:34.65668(3)	+53:41:17.0401(2)	-18.3(12.9)	2.6(16.3)	-14.6(12.7)	2.7(14.3)	2.9	0.2
1348+308	13:50:52.73618(5)	+30:34:53.5908(5)	-4.1(13.0)	12.6(11.0)	-6.7(12.5)	12.4(10.4)	0.9	0.2
1349-439	13:52:56.53457(16)	-44:12:40.3951(30)	0.8(9.5)	-32.3(15.1)	0.3(9.6)	-34.8(15.9)	2.3	2.4
1351-018	13:54:06.89537(14)	-02:06:03.1907(9)	4.4(1.3)	9.6(2.8)	4.4(1.3)	9.3(2.8)	0.3	0.3
1352-104	13:54:46.51870(3)	-10:41:02.6560(3)	2.7(5.9)	5.7(9.1)	2.8(5.8)	6.2(8.8)	0.5	0.9
1354+195	13:57:04.43663(1)	+19:19:07.3723(2)	0.9(7.9)	24.7(5.0)	-1.7(7.1)	21.1(5.1)	2.5	2.5
1354-174	13:57:06.07420(10)	-17:44:01.9045(8)	-23.3(26.9)	-68.5(35.6)	-23.6(26.8)	-58.1(31.4)	0.2	1.5
1354-152	13:57:11.24507(6)	-15:27:28.7866(7)	-2.1(3.9)	-1.6(5.8)	-2.0(4.1)	-1.4(6.1)	1.5	0.5
1402-012	14:04:45.89556(10)	-01:30:21.9464(21)	69.9(32.6)	20.2(30.7)	71.5(27.7)	21.0(30.5)	0.3	0.3
1402+044	14:05:01.11985(4)	+04:15:35.8190(5)	10.4(6.8)	-19.4(11.8)	10.7(6.5)	-17.8(11.2)	0.6	0.6
1406-076	14:08:56.48115(5)	-07:52:26.6669(4)	10.9(3.5)	-0.8(3.7)	11.1(3.4)	-0.6(3.7)	1.2	1.0
1416+067	14:19:08.18019(5)	+06:28:34.8040(14)	-53.5(50.3)	-13.6(73.8)	-36.1(30.5)	-4.2(58.2)	0.9	0.5
1418+546	14:19:46.59743(2)	+54:23:14.7871(2)	1.8(0.9)	-1.7(0.9)	1.9(0.9)	-1.6(0.9)	1.3	0.1
1417+385	14:19:46.61373(4)	+38:21:48.4758(5)	-2.8(1.4)	3.0(1.9)	-2.9(1.4)	3.0(1.9)	0.8	1.5
1417+273	14:19:59.29712(8)	+27:06:25.5499(23)	-49.3(18.7)	-7.5(21.1)	-52.2(17.8)	-10.1(22.9)	0.9	1.2
1423+146	14:25:49.01768(41)	+14:24:56.8999(56)	-8.8(6.9)	-5.0(14.1)	-8.5(7.0)	-5.8(13.9)	0.8	0.4
1424+366	14:26:37.08746(6)	+36:25:09.5725(8)	12.1(31.1)	-16.4(8.1)	13.0(28.9)	-16.5(8.6)	0.8	1.3
1424+240	14:27:00.39178(1)	+23:48:00.0371(2)	-9.9(18.4)	15.9(11.3)	-10.7(20.3)	17.3(12.7)	0.8	2.2
1424-418	14:27:56.29758(3)	-42:06:19.4374(3)	-10.1(1.6)	2.0(1.9)	-9.8(1.6)	2.0(1.8)	0.6	0.9
1428+422	14:30:23.74124(47)	+42:04:36.4941(37)	-27.5(31.9)	26.2(59.3)	-30.1(33.9)	27.4(57.1)	0.8	0.7
1428+370	14:30:40.58367(4)	+36:49:03.8883(6)	-18.8(10.3)	18.7(7.4)	-17.6(10.1)	18.7(7.7)	0.2	0.9
1430-178	14:32:57.69057(7)	-18:01:35.2485(7)	-69.6(55.7)	55.7(52.9)	-70.4(40.5)	46.4(26.1)	0.0	0.4
1432+200	14:34:39.79337(4)	+19:52:00.7357(4)	6.8(5.5)	-3.0(6.9)	7.5(5.3)	-3.7(7.3)	0.2	0.1
1435+638	14:36:45.80235(3)	+63:36:37.8671(2)	0.4(5.6)	3.4(12.1)	8.0(6.1)	6.6(12.0)	5.9	3.0
1435-218	14:38:09.46943(8)	-22:04:54.7480(5)	-9.5(8.6)	10.8(15.1)	-9.5(7.7)	11.4(15.2)	0.4	0.7
1441+252	14:43:56.89218(2)	+25:01:44.4905(7)	26.8(7.5)	-5.6(6.6)	26.1(8.1)	-5.5(5.9)	1.1	0.3
OQ172	14:45:16.46524(3)	+09:58:36.0732(5)	7.0(16.1)	-8.1(18.8)	6.1(14.7)	-4.2(18.2)	0.4	1.2
1443-162	14:45:53.37548(111)	-16:29:01.6243(65)	25.2(7.5)	-13.9(11.6)	24.6(7.6)	-13.7(12.1)	0.7	0.8
1445-161	14:48:15.05500(102)	-16:20:24.5442(60)	-31.0(32.1)	39.8(29.7)	-31.7(27.9)	44.5(29.0)	0.9	0.7
1451-375	14:54:27.40982(3)	-37:47:33.1446(3)	0.1(4.8)	7.2(10.5)	0.3(4.5)	6.3(10.1)	2.3	0.4
1451-400	14:54:32.91236(7)	-40:12:32.5142(6)	0.9(8.1)	-9.4(13.5)	-0.2(7.6)	-8.7(12.3)	0.1	0.4
1456+044	14:58:59.35608(12)	+04:16:13.8190(11)	-1.0(13.8)	-17.7(18.5)	0.2(13.0)	-19.2(15.1)	1.1	1.2
1459+480	15:00:48.65421(3)	+47:51:15.5377(3)	7.7(5.4)	-1.2(5.4)	7.9(5.5)	-1.4(5.3)	0.6	1.4
1502+106	15:04:24.97982(3)	+10:29:39.1988(14)	-2.2(1.3)	5.0(1.8)	-2.1(1.3)	4.9(1.8)	1.1	0.1
1502+036	15:05:06.47720(6)	+03:26:30.8129(7)	-1.2(3.7)	-0.6(3.5)	-1.3(3.4)	-0.4(3.6)	0.6	0.5

Table 7 continued

Table 7 (*continued*)

Name	Gaia 2015.0 Coordinates		VLBA PM		VLBA+Gaia PM		Gaia-VLBA Offset	
	RA (J2000)	Dec (J2000)	μ_α	μ_δ	μ_α	μ_δ	$\Delta\alpha$	$\Delta\delta$
			(h:m:s)	(d:m:s)	(mas yr $^{-1}$)	(mas yr $^{-1}$)	(σ)	(σ)
1510-089	15:12:50.53296(2)	-09:05:59.8294(2)	1.3(1.4)	-7.2(3.5)	1.4(1.5)	-6.9(3.6)	1.6	2.2
1511-100	15:13:44.89342(4)	-10:12:00.2650(3)	8.8(8.4)	-3.6(4.9)	8.4(7.8)	-3.3(5.2)	0.1	0.4
1514+197	15:16:56.79614(4)	+19:32:12.99921(3)	1.8(3.5)	-7.8(4.5)	2.0(3.2)	-8.4(4.5)	0.6	0.5
1514-241	15:17:41.81318(2)	-24:22:19.4769(2)	-4.8(2.9)	6.3(6.3)	-3.8(2.9)	-4.0(5.5)	3.1	5.4
1520+437	15:21:49.61389(5)	+43:36:39.2668(8)	-5.0(3.0)	6.5(5.5)	-5.1(3.0)	6.8(5.3)	0.2	1.8
1520+319	15:22:09.99173(3)	+31:44:14.3818(5)	-13.0(5.7)	4.9(5.5)	-12.3(5.7)	5.1(5.4)	0.1	0.4
1519-273	15:22:37.67595(7)	-27:30:10.7862(7)	7.0(1.5)	5.4(1.4)	6.9(1.4)	5.6(1.4)	0.7	1.0
1522+155	15:24:41.61148(4)	+15:21:21.0496(3)	25.8(19.3)	-36.3(51.1)	25.4(14.9)	-83.4(19.6)	0.4	2.7
1532+016	15:34:52.45367(4)	+01:31:04.2056(5)	-13.9(17.1)	-30.1(16.2)	-13.8(17.6)	-38.1(16.2)	0.1	1.4
1538+149	15:40:49.49099(7)	+14:47:45.8897(8)	6.4(4.5)	-14.0(5.2)	6.4(4.7)	-14.2(5.2)	7.5	6.4
1547+507	15:49:17.46857(5)	+50:38:05.7878(6)	12.6(5.5)	2.9(6.1)	12.4(5.4)	3.0(6.1)	0.0	0.6
1546+027	15:49:29.43687(3)	+02:37:01.1635(3)	4.4(2.3)	1.6(6.2)	4.3(2.2)	2.7(6.2)	0.8	0.6
1548+056	15:50:35.26926(4)	+05:27:10.4489(3)	-0.3(1.6)	9.6(2.8)	-0.2(1.6)	9.6(2.9)	0.4	1.1
1550-242	15:53:31.62785(6)	-24:22:06.0360(2)	1.1(15.9)	-37.3(56.7)	1.6(16.3)	-29.6(35.9)	0.7	1.3
1549-790	15:56:58.88092(48)	-79:14:04.2779(12)	-36.2(28.2)	-84.7(31.0)	37.3(65.6)	-71.3(33.6)	23.3	4.4
1555+001	15:57:51.43393(9)	-00:01:50.4135(8)	-1.9(2.9)	0.7(3.7)	-1.8(2.9)	1.0(3.6)	0.5	0.4
1554-643	15:58:50.28382(5)	-64:32:29.6281(3)	-2.1(12.5)	-2.8(36.8)	-88.5(32.8)	501.7(134.7)	10.6	31.6
1557+032	15:59:30.97263(14)	+03:04:48.2565(13)	1.0(4.1)	-17.5(5.8)	0.9(4.4)	-18.2(6.0)	0.1	0.1
1556-245	15:59:41.40911(5)	-24:42:38.8320(2)	33.3(51.6)	4.6(41.3)	42.1(44.4)	6.3(10.1)	0.3	0.2
1601+112	16:03:41.93128(2)	+11:05:48.6793(2)	-6.9(11.4)	10.9(19.1)	-6.8(9.6)	12.0(19.0)	1.4	0.8
1602-115	16:05:17.53166(5)	-11:39:26.8307(3)	2.6(8.2)	34.8(20.3)	2.6(8.9)	40.7(18.5)	0.0	1.3
1604-333	16:07:34.76231(6)	-33:31:08.9134(3)	8.6(14.2)	19.7(22.4)	8.5(15.1)	16.5(19.0)	0.4	0.5
1606+106	16:08:46.20318(3)	+10:29:07.7755(3)	5.4(0.9)	0.1(0.9)	5.4(1.0)	0.1(0.9)	0.3	0.8
1606-398	16:10:21.87911(8)	-39:58:58.3292(3)	-11.5(71.4)	-57.3(96.7)	-19.6(58.5)	-50.2(83.8)	0.0	1.0
1608+243	16:10:42.02677(3)	+24:14:49.0110(7)	2.8(8.5)	-13.0(5.5)	2.9(8.8)	-13.7(4.7)	0.3	0.9
1611-710	16:16:30.64150(11)	-71:08:31.4535(6)	3.5(23.3)	19.8(20.1)	3.4(22.2)	22.0(18.6)	0.0	1.2
1614+051	16:16:37.55684(8)	+04:59:32.7379(6)	5.8(3.4)	-6.4(3.5)	5.7(3.6)	-5.7(3.7)	0.2	2.3
1615+029	16:17:49.90811(2)	+02:46:43.1046(1)	-15.9(10.5)	-6.4(29.7)	-15.3(11.1)	-9.0(28.6)	0.2	1.6
1616+063	16:19:03.68771(4)	+06:13:02.2427(3)	-18.6(7.9)	-4.9(10.7)	-16.8(7.6)	-6.4(10.4)	1.1	0.6
1617+229	16:19:14.82485(24)	+22:47:47.8516(12)	-3.0(4.5)	-28.2(6.3)	-2.7(4.6)	-28.4(6.5)	1.1	0.6
1619-680	16:24:18.43694(2)	-68:09:12.4960(1)	-4.6(14.3)	24.2(18.2)	-6.3(14.2)	29.0(18.1)	2.5	3.5
1622-253	16:25:46.89120(358)	-25:27:38.3264(78)	-0.3(1.1)	7.8(1.4)	-0.2(1.1)	8.0(1.4)	0.1	0.1
1622-297	16:26:06.02085(4)	-29:51:26.9712(3)	-4.3(6.4)	-17.3(6.7)	-4.1(6.0)	-16.2(6.9)	0.4	0.8
1624-617	16:28:54.68978(8)	-61:52:36.3987(4)	-14.5(10.7)	-5.6(18.6)	-16.1(11.9)	-6.8(18.6)	0.1	1.6
1633+38	16:35:15.49296(2)	+38:08:04.5004(3)	6.9(1.5)	2.2(2.7)	7.1(1.6)	2.3(2.9)	1.3	0.8
1636+473	16:37:45.13043(7)	+47:17:33.8315(7)	-7.0(5.2)	21.7(6.2)	-7.2(5.0)	20.8(6.9)	1.8	0.4
1637+574	16:38:13.45631(3)	+57:20:23.9788(3)	5.3(1.7)	-1.6(2.2)	5.3(1.7)	-1.8(2.2)	0.2	0.7
NRAO512	16:40:29.63280(6)	+39:46:46.0283(7)	-1.2(0.6)	-2.8(0.6)	-1.2(0.6)	-2.9(0.6)	0.4	0.2
1639+230	16:41:25.22761(3)	+22:57:04.0331(5)	0.3(2.8)	-7.1(5.0)	0.4(2.8)	-7.3(4.8)	1.6	0.8
1642+690	16:42:07.84806(87)	+68:56:39.7548(36)	6.2(1.7)	-19.0(3.2)	6.3(1.6)	-19.3(3.0)	0.5	0.4
1633-810	16:42:57.34553(26)	-81:08:35.0705(4)	13.3(18.1)	-9.2(24.9)	15.2(17.0)	-10.4(22.4)	0.3	0.5
1651+391	16:52:58.50957(11)	+39:02:49.8227(18)	4.5(6.5)	-25.0(8.2)	4.9(5.6)	-25.5(7.9)	0.1	0.3
DA426	16:53:52.21715(2)	+39:45:36.6065(2)	-1.7(1.9)	2.7(2.8)	0.1(2.0)	1.7(3.0)	25.5	10.1
1656+348	16:58:01.41920(2)	+34:43:28.4018(3)	15.4(17.8)	-13.9(24.1)	10.9(8.3)	-16.7(18.2)	0.4	0.4
1656+477	16:58:02.77963(2)	+47:37:49.2304(4)	1.3(11.4)	-17.2(17.5)	3.1(10.4)	-19.6(17.8)	1.7	0.7
1655+077	16:58:09.01129(10)	+07:41:27.5398(15)	-4.4(10.2)	-8.8(11.1)	-5.3(9.8)	-8.5(10.8)	1.6	0.4
1656+053	16:58:33.44731(2)	+05:15:16.4437(2)	-20.3(15.0)	-6.1(9.7)	-20.0(14.0)	-8.3(8.7)	0.2	1.0

Table 7 continued

Table 7 (continued)

Name	Gaia 2015.0 Coordinates		VLBA PM		VLBA+Gaia PM		Gaia-VLBA Offset	
	RA (J2000) (h:m:s)	Dec (J2000) (d:m:s)	μ_α	μ_δ	μ_α	μ_δ	$\Delta\alpha$	$\Delta\delta$
			(μ as yr $^{-1}$)	(σ)	(σ)			
1656-075	16:58:44.06183(4)	-07:39:17.6944(4)	-55.0(26.1)	-62.2(22.0)	-56.3(24.9)	-62.9(21.8)	3.5	0.2
1657-261	17:00:53.15405(2)	-26:10:51.7250(4)	-3.2(3.6)	7.3(5.1)	-3.2(3.6)	7.6(5.7)	0.7	1.0
1659+399	17:01:24.63485(2)	+39:54:37.0914(3)	-3.9(12.2)	-3.5(10.0)	-2.1(11.7)	-3.8(8.8)	1.6	0.5
1657-562	17:01:44.85821(20)	-56:21:55.9045(13)	34.0(10.1)	-109.1(17.8)	33.7(10.1)	-110.7(17.0)	0.4	1.2
1659-621	17:03:36.54128(5)	-62:12:40.0082(3)	-32.1(9.4)	-28.1(12.7)	-30.3(9.5)	-25.3(12.9)	1.7	1.6
1705+456	17:07:17.75343(2)	+45:36:10.5530(3)	-60.6(20.3)	27.4(16.2)	-41.0(12.5)	25.5(11.6)	4.2	0.6
1705+018	17:07:34.41524(3)	+01:48:45.6995(3)	-1.6(2.8)	-12.0(4.8)	-1.2(2.7)	-11.7(5.0)	1.2	1.0
1705+135	17:07:45.63729(2)	+13:31:05.2326(2)	-16.3(25.4)	-0.8(21.5)	-15.0(18.0)	-2.8(14.1)	1.7	1.2
1706-174	17:09:34.34555(14)	-17:28:53.3651(16)	-3.7(7.0)	0.5(7.4)	-4.0(6.8)	-0.4(7.4)	1.1	0.0
1717+178	17:19:13.04837(7)	+17:45:06.4389(14)	-5.6(3.0)	-1.4(3.9)	-5.8(2.9)	-0.9(4.2)	1.6	1.2
1722+330	17:24:14.19793(22)	+33:03:03.9451(28)	-22.3(11.0)	29.9(23.5)	-22.6(10.3)	29.6(21.6)	0.5	2.1
1726+455	17:27:27.65081(2)	+45:30:39.7313(3)	-4.4(1.0)	-3.0(0.9)	-4.4(1.0)	-2.9(0.9)	0.6	0.3
1725+123	17:28:07.05124(4)	+12:15:39.4852(11)	1.3(11.4)	-12.2(20.5)	0.7(10.8)	-12.3(20.9)	0.5	0.3
1727+502	17:28:18.62394(2)	+50:13:10.4704(2)	110.0(43.0)	-62.3(39.5)	-20.0(13.6)	-5.3(17.2)	7.1	3.9
1725+044	17:28:24.95276(2)	+04:27:04.9142(3)	7.4(8.6)	8.5(17.9)	9.8(7.2)	12.0(15.4)	1.5	1.0
NRAO530	17:33:02.70719(365)	-13:04:49.5301(464)	7.4(1.3)	7.1(2.3)	7.4(1.3)	7.2(2.3)	0.4	0.4
1725-795	17:33:40.70045(21)	-79:35:55.7166(3)	12.0(13.0)	-1.9(27.3)	11.3(12.9)	-1.4(21.5)	0.8	0.1
1732+389	17:34:20.57854(6)	+38:57:51.4405(10)	-4.7(3.2)	4.7(4.2)	-4.7(3.1)	4.7(4.4)	0.1	2.6
1734+363	17:35:48.08670(6)	+36:16:45.6116(10)	-19.9(12.4)	0.7(9.2)	-18.6(13.4)	0.7(9.9)	1.7	0.0
1736+324	17:38:40.50183(2)	+32:24:09.0255(3)	1.2(11.0)	-20.3(17.6)	1.3(12.1)	-20.3(18.7)	0.6	0.1
1738+499	17:39:27.39046(4)	+49:55:03.3671(7)	-0.6(6.1)	-0.8(5.9)	-0.1(6.4)	-0.6(5.7)	0.7	2.0
1738+476	17:39:57.12918(7)	+47:37:58.3589(14)	-4.1(4.7)	3.7(4.6)	-4.4(4.5)	3.7(5.0)	1.7	1.9
1741-038	17:43:58.85615(3)	-03:50:04.6173(5)	1.0(0.5)	-0.7(0.5)	1.0(0.5)	-0.6(0.6)	0.4	1.1
NGC6454	17:44:56.60639(28)	+55:42:17.1553(29)	-13.5(11.1)	1.6(8.8)	-14.6(12.1)	0.1(10.2)	2.4	2.0
1743+173	17:45:35.20822(5)	+17:20:01.4234(10)	6.8(4.4)	0.7(12.3)	6.6(4.5)	0.8(11.7)	0.9	0.3
1745+624	17:46:14.03493(85)	+62:26:54.7314(80)	10.8(1.4)	10.7(2.2)	10.7(1.5)	10.4(2.2)	0.9	0.9
1749+701	17:48:32.84033(4)	+70:05:50.7691(4)	10.7(10.5)	8.2(6.3)	7.2(10.2)	8.8(6.4)	0.5	0.4
1749+096	17:51:32.81859(1)	+09:39:00.7287(3)	0.5(0.5)	-0.1(0.5)	0.4(0.5)	-0.0(0.5)	0.9	1.2
1751+441	17:53:22.64790(9)	+44:09:45.6866(9)	-43.6(8.2)	-0.1(11.4)	-42.8(8.6)	-2.0(11.8)	0.6	0.4
1751+288	17:53:42.47365(3)	+28:48:04.9389(7)	-5.9(3.9)	-1.7(3.3)	-6.3(3.7)	-1.4(3.1)	0.3	0.0
1754+159	17:56:33.72564(4)	+15:53:43.8331(15)	-2.3(19.4)	-21.2(17.6)	-1.6(16.3)	-19.5(15.4)	0.8	0.1
1758+388	18:00:24.76534(3)	+38:48:30.6970(3)	-1.7(2.3)	1.5(4.6)	-1.7(2.3)	2.1(4.4)	1.0	1.6
1803+784	18:00:45.68383(7)	+78:28:04.0180(3)	-0.1(0.5)	-0.8(0.4)	-0.1(0.4)	-0.8(0.4)	1.0	1.4
1800+440	18:01:32.31482(3)	+44:04:21.8997(4)	-2.8(3.7)	-4.8(6.1)	-2.9(3.8)	-4.3(6.2)	0.2	1.4
1758-651	18:03:23.49663(6)	-65:07:36.7610(5)	3.4(6.0)	-0.9(7.6)	3.3(6.3)	-1.1(7.7)	0.3	0.7
3C371	18:06:50.68048(5)	+69:49:28.1082(3)	6.8(0.8)	-0.3(0.6)	6.7(0.8)	-0.3(0.6)	3.8	1.1
1826+796	18:23:14.10883(225)	+79:38:49.0054(30)	39.9(33.1)	-24.0(19.8)	44.4(37.0)	-19.5(23.1)	0.0	1.3
1823+689	18:23:32.85372(26)	+68:57:52.6113(24)	4.4(6.1)	-0.6(9.2)	3.9(6.1)	-0.8(8.7)	0.7	0.5
1821+107	18:24:02.85527(2)	+10:44:23.7739(3)	-8.9(5.5)	20.1(10.8)	-8.3(5.5)	17.7(8.4)	1.1	0.8
1823+568	18:24:07.06827(3)	+56:51:01.4885(3)	-4.5(1.4)	2.5(2.0)	-4.7(1.4)	2.1(1.9)	3.3	7.1
1824-582	18:29:12.40234(26)	-58:13:55.1622(16)	-21.5(13.0)	-33.4(23.5)	-21.5(13.2)	-34.1(23.2)	0.0	0.2
1830+285	18:32:50.18566(2)	+28:33:35.9553(4)	-11.7(9.3)	10.9(10.6)	-9.1(7.7)	11.0(9.3)	2.4	0.2
1831-711	18:37:28.71498(3)	-71:08:43.5549(2)	6.0(4.8)	-13.4(5.7)	5.9(4.7)	-13.7(5.6)	0.6	1.1
3C390.3	18:42:08.98958(13)	+79:46:17.1283(1)	40.1(25.6)	-0.8(26.4)	9.5(19.4)	2.1(9.9)	4.1	0.7
1842+681	18:42:33.64189(17)	+68:09:25.2279(21)	1.3(3.9)	-2.2(4.7)	2.0(3.8)	-2.3(4.3)	1.2	0.1
1842-289	18:45:51.36825(16)	-28:52:40.2749(27)	-1.0(807.0)	7.9(1300.7)	1.4(813.7)	8.4(1242.4)	0.2	0.5
1846+322	18:48:22.08856(3)	+32:19:02.6034(6)	-29.4(5.2)	7.6(5.7)	-29.5(4.7)	7.2(5.9)	0.2	0.7

Table 7 continued

Table 7 (*continued*)

Name	Gaia 2015.0 Coordinates		VLBA PM		VLBA+Gaia PM		Gaia-VLBA Offset	
	RA (J2000)	Dec (J2000)	μ_α	μ_δ	μ_α	μ_δ	$\Delta\alpha$	$\Delta\delta$
			(h:m:s)	(d:m:s)	(mas yr $^{-1}$)	(mas yr $^{-1}$)	(σ)	(σ)
1849+670	18:49:16.07223(4)	+67:05:41.6802(4)	-0.9(1.2)	-4.3(1.6)	-0.9(1.2)	-4.3(1.5)	1.4	0.2
1856+736	18:54:57.29993(5)	+73:51:19.9064(3)	-5.2(10.8)	-37.0(12.7)	-2.6(9.3)	-40.0(11.5)	0.6	0.5
3C395	19:02:55.93890(2)	+31:59:41.7013(3)	68.6(10.2)	-31.7(7.6)	66.2(9.9)	-32.1(6.9)	2.6	0.1
1908+484	19:09:46.56265(18)	+48:34:31.8192(26)	-48.8(78.7)	18.4(47.0)	-48.0(82.3)	20.4(51.4)	0.4	0.4
1908-201	19:11:09.65290(4)	-20:06:55.1084(7)	4.8(1.5)	-5.4(2.8)	4.8(1.6)	-5.1(3.0)	0.2	1.2
1903-802	19:12:40.01946(18)	-80:10:05.9460(7)	-22.4(12.0)	-17.9(13.6)	-7.1(12.3)	-15.0(11.0)	2.6	1.0
1920-211	19:23:32.18983(3)	-21:04:33.3330(5)	-6.7(3.6)	-1.4(6.3)	-6.8(3.8)	-1.4(6.1)	0.5	0.3
1921-293	19:24:51.05600(3)	-29:14:30.1191(5)	-4.8(0.9)	10.0(1.5)	-4.8(1.0)	10.0(1.5)	1.8	3.9
1923+210	19:25:59.60535(12)	+21:06:26.1625(14)	10.1(2.2)	17.8(1.4)	10.0(2.4)	17.9(1.4)	0.1	0.3
1928+738	19:27:48.49505(6)	+73:58:01.5709(2)	-2.2(3.6)	-5.8(11.5)	-3.1(3.2)	-3.9(11.3)	1.8	4.3
1925-610	19:30:06.16021(11)	-60:56:09.1836(9)	0.9(12.0)	8.3(14.2)	0.6(12.5)	7.5(15.8)	1.1	0.7
1929-457	19:32:44.88773(5)	-45:36:37.9287(4)	-22.8(86.4)	5.2(251.1)	-18.4(54.1)	2.4(29.2)	0.2	0.1
1933-400	19:37:16.21733(2)	-39:58:01.5530(2)	21.1(6.8)	-7.4(9.1)	20.8(5.8)	-6.8(9.0)	1.4	0.6
1936-155	19:39:26.65775(7)	-15:25:43.0581(10)	8.0(2.3)	2.2(3.8)	8.1(2.1)	2.1(4.3)	0.1	0.4
1937-101	19:39:57.25659(3)	-10:02:41.5208(5)	39.5(11.6)	41.9(17.2)	38.4(11.2)	37.8(14.4)	0.2	1.4
1935-692	19:40:25.52824(6)	-69:07:56.9717(16)	-31.2(8.4)	-10.5(12.4)	-30.5(9.2)	-9.7(12.4)	1.7	0.0
1947+079	19:50:05.53994(17)	+08:07:13.9772(16)	31.8(64.0)	-15.9(118.0)	33.9(60.4)	-19.8(67.1)	0.2	2.2
1954+513	19:55:42.73826(4)	+51:31:48.5458(4)	-2.1(8.1)	-1.8(4.1)	-1.2(7.9)	-2.1(4.2)	0.0	0.8
1954-388	19:57:59.81991(28)	-38:45:06.3544(8)	3.3(1.3)	-8.5(1.8)	3.1(1.3)	-8.7(1.9)	2.3	2.0
1958-179	20:00:57.09044(3)	-17:48:57.6726(2)	-7.8(1.0)	-3.9(1.3)	-7.7(1.0)	-4.0(1.4)	0.2	0.5
2000+472	20:02:10.41828(13)	+47:25:28.7741(10)	-15.4(3.8)	-4.4(3.0)	-15.9(3.8)	-4.2(3.0)	0.3	0.3
2000+148	20:02:41.99806(298)	+15:01:14.5675(170)	0.0(6.5)	25.6(14.8)	0.0(6.0)	24.1(15.0)	0.4	0.4
2000-330	20:03:24.11635(2)	-32:51:45.1336(2)	51.6(18.1)	-50.5(45.9)	42.4(13.5)	-67.2(24.1)	1.4	1.0
2007+777	20:05:30.99856(7)	+77:52:43.2475(2)	22.8(2.9)	-0.0(1.5)	22.8(3.0)	-0.0(1.5)	1.3	0.1
2005+403	20:07:44.94473(4)	+40:29:48.6042(5)	25.5(63.2)	-29.9(86.1)	-28.3(27.7)	-13.2(22.0)	3.5	0.6
2005-489	20:09:25.39062(2)	-48:49:53.7227(2)	20.4(61.4)	14.6(27.2)	-24.2(24.8)	-70.2(14.8)	5.4	9.3
2008-159	20:11:15.71090(4)	-15:46:40.2538(4)	-6.5(2.4)	12.5(3.3)	-6.2(2.4)	12.4(3.3)	0.7	0.2
2017+743	20:17:13.07924(8)	+74:40:48.0001(4)	-7.3(9.9)	7.1(7.0)	-8.2(8.9)	7.8(6.6)	0.6	0.4
2021+614	20:22:06.68334(50)	+61:36:58.8110(41)	16.5(9.4)	16.7(12.8)	18.6(9.2)	17.2(12.5)	3.1	1.4
2021+317	20:23:19.01734(3)	+31:53:02.3053(5)	9.6(15.3)	12.9(13.2)	9.9(14.0)	9.2(11.6)	0.3	2.0
2029+024	20:31:47.25116(9)	+02:39:37.2832(12)	5.8(81.2)	17.4(109.1)	6.0(53.3)	17.6(73.1)	0.4	0.4
2030+547	20:31:47.95853(3)	+54:55:03.1384(3)	3.6(20.2)	15.4(41.2)	3.1(15.0)	-16.2(29.9)	0.4	4.6
2029+121	20:31:54.99417(33)	+12:19:41.3394(29)	-10.3(3.6)	-18.0(4.3)	-10.7(3.5)	-17.6(4.3)	0.3	0.2
3C418	20:38:37.03465(13)	+51:19:12.6621(14)	-15.4(1.3)	-7.8(1.5)	-15.3(1.2)	-7.7(1.6)	0.6	0.3
2037-253	20:40:08.77296(4)	-25:07:46.6633(4)	11.4(20.6)	-56.9(12.1)	16.3(17.4)	-49.7(10.7)	0.5	1.5
CL4	20:50:51.13148(4)	+31:27:27.3753(12)	-27.9(33.6)	17.2(51.8)	-17.7(17.2)	20.6(48.8)	0.6	1.0
2051+745	20:51:33.73450(14)	+74:41:40.4984(6)	-21.0(34.3)	7.3(17.7)	-22.8(21.5)	7.9(11.0)	0.1	0.2
2052-474	20:56:16.35981(3)	-47:14:47.6275(4)	-12.9(2.7)	-4.1(3.5)	-12.9(2.7)	-4.4(3.5)	0.1	0.5
2054-377	20:57:41.60358(12)	-37:34:02.9908(15)	38.4(15.4)	34.5(27.1)	36.8(18.4)	31.2(27.0)	0.7	0.4
2058-297	21:01:01.66000(7)	-29:33:27.8363(8)	-5.1(79.1)	-7.7(59.0)	0.2(59.8)	-8.4(32.5)	0.2	0.1
2059+034	21:01:38.83419(2)	+03:41:31.3207(3)	-5.5(3.3)	-25.0(3.7)	-5.3(3.5)	-25.0(3.8)	1.5	0.2
2106+143	21:08:41.03215(9)	+14:30:27.0147(15)	-4.1(3.8)	6.7(6.3)	-4.0(4.3)	6.9(6.2)	0.1	1.4
2106-413	21:09:33.18903(10)	-41:10:20.6079(16)	5.0(9.9)	-7.1(10.5)	5.3(9.5)	-7.8(11.1)	4.1	1.5
2113+293	21:15:29.41337(11)	+29:33:38.3666(14)	-0.1(1.1)	0.0(1.7)	-0.1(1.2)	0.1(1.7)	0.7	0.3
2109-811	21:16:30.84542(169)	-80:53:55.2263(72)	1.8(13.0)	7.7(15.2)	2.0(13.7)	8.1(15.3)	0.3	0.4
2123-463	21:26:30.70416(3)	-46:05:47.8924(4)	-4.3(20.4)	-5.4(35.5)	-8.3(21.1)	-5.2(33.1)	3.8	0.6
2126-158	21:29:12.17590(2)	-15:38:41.0412(4)	-10.8(2.3)	-66.4(4.8)	-10.6(2.5)	-66.5(5.2)	0.7	2.1

Table 7 continued

Table 7 (continued)

Name	Gaia 2015.0 Coordinates		VLBA PM		VLBA+Gaia PM		Gaia-VLBA Offset	
	RA (J2000) (h:m:s)	Dec (J2000) (d:m:s)	μ_α	μ_δ	μ_α	μ_δ	$\Delta\alpha$	$\Delta\delta$
			(μ as yr $^{-1}$)	(σ)	(σ)			
2127-096	21:30:19.08827(3)	-09:27:37.4358(9)	18.8(8.6)	7.4(11.9)	18.3(8.7)	5.4(11.7)	0.0	0.7
2134+00	21:36:38.58640(2)	+00:41:54.2120(4)	-6.1(4.3)	-54.3(4.1)	-5.0(4.3)	-54.4(3.9)	4.9	0.2
2135-184	21:38:41.92612(40)	-18:10:44.3249(70)	-1190.4(1986.6)	-218.0(1587.8)	-1184.9(2107.3)	-273.2(2386.7)	1.6	7.5
2136+141	21:39:01.30925(4)	+14:23:35.9916(5)	2.5(1.9)	1.6(1.8)	2.7(1.8)	1.5(1.9)	0.5	1.4
2142+110	21:45:18.77510(4)	+11:15:27.3116(7)	-2.6(10.9)	-5.7(11.8)	-1.9(10.7)	-5.5(13.4)	0.8	1.0
2144+092	21:47:10.16296(4)	+09:29:46.6721(6)	4.9(5.8)	-5.4(4.8)	5.3(5.8)	-5.7(4.7)	0.3	0.3
2142-758	21:47:12.73075(5)	-75:36:13.2252(3)	48.9(18.7)	14.7(10.8)	48.9(18.3)	15.2(10.7)	2.5	1.0
2146-783	21:52:03.15353(25)	-78:07:06.6332(10)	3.9(65.5)	70.4(31.5)	-36.3(63.1)	119.3(30.7)	4.2	5.5
2155-152	21:58:06.28183(2)	-15:01:09.3296(6)	-29.9(6.6)	-40.6(7.4)	-30.4(6.3)	-40.1(7.3)	1.8	1.5
2155-304	21:58:52.06513(2)	-30:13:32.1182(4)	11.1(7.4)	8.2(20.6)	12.4(7.6)	7.9(18.7)	0.2	0.2
VR422201	22:02:43.29137(2)	+42:16:39.9796(2)	-1.9(1.4)	2.0(2.3)	-2.1(1.5)	1.5(2.3)	0.1	2.0
2204-540	22:07:43.73328(2)	-53:46:33.8200(4)	-4.9(6.9)	-16.7(10.1)	-5.1(6.7)	-16.2(9.6)	0.3	0.1
2205+166	22:07:52.86568(5)	+16:52:17.8140(9)	-14.9(15.5)	9.7(29.2)	-15.2(14.9)	7.8(25.5)	0.1	1.6
2208-137	22:11:24.09946(2)	-13:28:09.7238(4)	2.6(17.6)	16.3(51.4)	2.7(18.1)	16.4(45.9)	0.2	0.0
2209+236	22:12:05.96642(6)	+23:55:40.5439(5)	21.7(2.0)	2.5(1.8)	21.7(2.0)	2.6(2.0)	1.6	0.1
2210-257	22:13:02.49789(6)	-25:29:30.0812(11)	-4.4(17.0)	-10.3(53.2)	-17.5(16.0)	-20.3(47.6)	1.6	0.5
2214+350	22:16:20.00993(2)	+35:18:14.1804(3)	5.6(3.1)	-69.9(5.1)	5.6(3.1)	-69.5(5.0)	1.3	2.4
2215+150	22:18:10.91387(4)	+15:20:35.7170(6)	5.4(4.7)	1.2(5.0)	5.6(4.8)	1.1(5.5)	0.9	0.7
2216-038	22:18:52.03772(2)	-03:35:36.8791(3)	0.7(2.8)	11.4(4.8)	0.5(2.4)	11.0(4.5)	0.3	0.8
2220-351	22:23:05.93055(2)	-34:55:47.1778(2)	-11.2(13.7)	25.2(35.0)	-12.0(13.9)	22.8(33.9)	0.2	0.2
3C446	22:25:47.25956(5)	-04:57:01.3922(12)	0.2(1.3)	10.9(1.1)	0.3(1.3)	10.9(1.1)	5.0	1.2
2227-088	22:29:40.08435(2)	-08:32:54.4359(4)	-5.4(2.8)	6.9(3.5)	-5.2(2.8)	7.1(3.6)	0.6	0.8
2229+695	22:30:36.46931(31)	+69:46:28.0763(11)	39.4(3.1)	4.8(1.7)	39.3(3.3)	4.8(1.6)	1.5	0.5
2232-488	22:35:13.23659(2)	-48:35:58.7942(5)	17.3(11.7)	4.0(9.8)	16.0(10.8)	4.0(9.3)	0.5	0.7
2235+731	22:36:38.59473(302)	+73:22:52.6492(165)	5.2(9.1)	16.9(10.9)	5.1(9.4)	17.8(11.5)	0.8	0.8
2236-572	22:39:12.07652(117)	-57:01:00.8440(81)	-3.7(10.3)	-23.6(15.8)	-3.9(10.3)	-23.1(14.3)	0.5	0.6
2239+096	22:41:49.71729(5)	+09:53:52.4451(5)	18.4(33.5)	28.4(27.8)	19.0(29.7)	31.0(27.6)	0.5	0.1
2243+047	22:45:53.65414(5)	+05:00:56.9617(6)	-9.4(11.1)	16.8(26.2)	-9.6(11.8)	14.3(25.2)	0.6	0.8
2245-328	22:48:38.68573(3)	-32:35:52.1887(4)	-5.4(10.8)	-2.8(16.9)	-5.2(11.4)	-4.1(15.7)	0.3	1.2
2250+194	22:53:07.36913(2)	+19:42:34.6280(2)	3.9(3.7)	-8.2(7.8)	3.8(3.4)	-9.5(8.3)	1.8	3.2
2253+417	22:55:36.70783(6)	+42:02:52.5322(4)	-4.6(7.9)	-16.3(10.0)	-5.2(8.5)	-16.6(9.5)	0.2	0.7
2254+074	22:57:17.30307(4)	+07:43:12.3018(4)	-2.8(3.1)	11.7(4.2)	-2.8(3.0)	11.3(4.2)	1.2	2.1
2254+024	22:57:17.56310(4)	+02:43:17.5121(7)	5.8(9.5)	-21.4(19.2)	4.8(9.3)	-20.8(18.1)	0.1	0.8
2255-282	22:58:05.96288(2)	-27:58:21.2569(3)	-4.6(1.2)	1.7(2.0)	-4.5(1.2)	2.0(2.1)	0.1	0.3
2300-683	23:03:43.56467(4)	-68:07:37.4443(3)	49.3(12.0)	-67.0(13.0)	48.7(12.5)	-68.9(15.0)	1.1	3.8
2302+232	23:04:36.43643(7)	+23:31:07.6111(8)	-3.0(6.7)	7.5(18.2)	-2.9(6.5)	8.1(16.5)	0.3	0.1
2306-312	23:09:14.33134(4)	-30:59:12.5842(5)	17.3(26.3)	-10.8(89.5)	14.2(19.1)	-8.8(38.6)	1.7	0.5
2309+454	23:11:47.40909(14)	+45:43:56.0162(6)	0.3(5.4)	-6.6(7.2)	0.4(5.9)	-6.7(7.3)	0.8	0.4
2312-319	23:14:48.50058(3)	-31:38:39.5265(4)	-51.3(30.5)	-23.9(48.9)	-37.1(20.0)	-21.1(32.6)	1.2	0.3
2314-340	23:16:43.38633(3)	-33:49:12.4916(7)	67.2(106.5)	-141.3(103.1)	-15.7(33.2)	-526.4(62.2)	2.7	6.4
2318+049	23:20:44.85666(3)	+05:13:49.9524(3)	-5.0(1.7)	-1.7(1.5)	-5.2(1.9)	-1.5(1.6)	2.2	0.6
2319+317	23:21:54.95595(6)	+32:04:07.6228(4)	1.4(3.4)	-9.0(4.9)	1.2(3.4)	-8.8(4.7)	0.8	0.9
2320+506	23:22:25.98222(9)	+50:57:51.9642(6)	12.8(5.8)	12.4(16.6)	12.8(5.5)	13.6(14.9)	0.3	0.6
2320-035	23:23:31.95375(3)	-03:17:05.0242(3)	-4.5(13.8)	1.5(13.6)	-4.0(11.9)	-3.8(10.8)	0.0	1.1
2321-375	23:24:07.11184(4)	-37:14:22.4553(5)	66.1(52.0)	1.0(37.6)	55.5(28.2)	9.5(20.2)	0.8	1.1
2325+093	23:27:33.58051(4)	+09:40:09.4621(4)	4.9(30.4)	-16.4(19.0)	4.5(32.7)	-17.4(19.7)	1.1	1.7
2325-150	23:27:47.96439(7)	-14:47:55.7501(8)	-14.5(41.4)	32.9(21.2)	-0.8(29.8)	39.7(16.6)	2.1	0.7

Table 7 continued

Table 7 (*continued*)

Name	Gaia 2015.0 Coordinates		VLBA PM		VLBA+Gaia PM		Gaia-VLBA Offset	
	RA (J2000)	Dec (J2000)	μ_α	μ_δ	μ_α	μ_δ	$\Delta\alpha$	$\Delta\delta$
			(h:m:s)	(d:m:s)	(mas yr $^{-1}$)	(mas yr $^{-1}$)	(σ)	(σ)
2326-477	23:29:17.70428(2)	-47:30:19.1146(2)	2.6(7.8)	22.0(10.3)	1.5(8.4)	21.9(9.9)	4.5	1.3
2328+107	23:30:40.85225(7)	+11:00:18.7091(6)	-12.5(14.9)	-4.3(27.8)	-12.5(18.1)	-6.6(23.4)	0.1	1.2
2329-384	23:31:59.47612(2)	-38:11:47.6505(3)	12.3(9.1)	-30.9(11.1)	10.8(8.6)	-30.6(11.2)	1.7	1.5
2331-240	23:33:55.23785(2)	-23:43:40.6588(3)	-5.8(11.5)	-24.6(15.0)	-0.9(9.4)	-28.1(13.2)	1.5	1.7
2333-415	23:36:33.98507(9)	-41:15:21.9842(5)	-14.1(11.6)	-0.6(34.2)	-13.2(11.1)	-3.3(34.9)	0.1	0.4
2335-027	23:37:57.33915(8)	-02:30:57.6295(7)	-5.5(4.7)	-6.5(6.3)	-5.8(4.7)	-7.6(6.4)	1.0	0.2
2344+09A	23:46:36.83852(1)	+09:30:45.5144(1)	2.4(18.4)	-0.9(20.3)	-1.9(13.7)	-14.5(12.9)	2.6	4.9
2344-514	23:47:19.86409(3)	-51:10:36.0646(7)	8.4(15.7)	31.2(34.3)	8.4(15.7)	34.9(34.8)	0.3	1.0
2345-167	23:48:02.60851(3)	-16:31:12.0226(2)	-14.4(6.9)	-8.3(12.2)	-14.3(6.4)	-10.5(9.6)	0.2	1.0
2351-154	23:54:30.19516(3)	-15:13:11.2138(3)	-9.3(5.6)	4.6(11.3)	-9.5(6.0)	3.6(11.4)	0.2	2.5
2353-686	23:56:00.68137(6)	-68:20:03.4716(2)	9.6(8.8)	-8.4(9.0)	9.6(8.6)	-7.1(9.0)	0.8	1.9
2354-117	23:57:31.19757(2)	-11:25:39.1771(1)	-2.1(325.8)	-59.9(682.2)	-0.5(140.5)	-40.3(261.4)	0.4	3.3
2355-534	23:57:53.26600(3)	-53:11:13.6898(3)	-18.6(7.2)	-12.6(12.7)	-19.2(6.8)	-13.8(11.8)	2.0	1.0
2355-106	23:58:10.88237(3)	-10:20:08.6117(1)	-8.0(3.2)	-0.4(3.4)	-8.1(3.3)	-0.9(3.5)	0.9	2.4
2356+385	23:59:33.18072(23)	+38:50:42.3186(6)	4.1(1.5)	-6.0(2.3)	3.8(1.5)	-6.0(2.3)	0.4	0.6

NOTE—The *Gaia* coordinates are for epoch 2015.0, expressed in the J2000 reference frame. The *Gaia*-VLBA offsets are expressed in standard deviations of the *Gaia* astrometry from the VLBA time series fit, assuming that the error is dominated by the sole *Gaia* epoch in each coordinate.